Development, design and construction of a measuring station for momentum spectrometry of low-energy particle sources

Bachelor-Thesis

Julian Rausch

14.12.2021

Reviewers:

Dr. Oliver Meusel
Prof. Dr. Holger Podlech

Institut für Angewandte Physik
Goethe-Universität Frankfurt am Main

Erklärung nach § 30 (12) Ordnung für den Bachelor- und den Masterstudiengang

Hiermit erkläre ich, dass ich die Arbeit selbstständig und ohne Benutzung anderer als der angegebenen Quellen und Hilfsmittel verfasst habe. Alle Stellen der Arbeit, die wörtlich oder sinngemäß aus Veröffentlichungen oder aus anderen fremden Texten entnommen wurden, sind von mir als solche kenntlich gemacht worden. Ferner erkläre ich, dass die Arbeit nicht - auch nicht auszugsweise - für eine andere Prüfung verwendet wurde.

Frankfurt, den 14.12.2021

Contents

0.1 Introduction

In many fields of physics, experiments with charged particles are of great importance. Almost always, the processes studied depend on the energy of the particles. If the motion of the particles is directional, a momentum spectrometer can be used to determine the momentum of the particles when the charge is known. In addition, if the mass of the particles is known, the velocity and kinetic energy can be obtained.

Within the research for this thesis, a momentum spectrometer was set up and first measurements on accelerated ions were carried out.

For this purpose, the equipment for operating the spectrometer and for high-precision measurements was assembled. A control system that operates all used devices within a network and enables automatic measurements with the spectrometer was developed and the spectrometer was set up at a beamline that allows experiments with both a highly charged ion beam and ions from a Gabor lens.

The Gabor lens is an element that can be used for focusing and space charge compensation of highly charged ion beams. In the field of interaction with ion beams, many effects and properties of Gabor lenses can be studied experimentally. The measurements conducted show expected results for the energy distribution of the beam and for the spectrum of the ions from the Gabor lens as well as new insights into its effects on the ion beam, in particular with respect to charge change processes.

In addition, the setup provides the foundation for upcoming more extensive measurements on the combination of beam and Gabor lens to further investigate the influences of the beam on the parameters of the Gabor lens.

Finally, a number of assumptions and questions have been evolved, which can be tested and clarified by further measurements in the future.

Chapter 1

Beamline setup

A beam of positively charged ions is provided by an ion source. In order to transport the ion beam from the source to the experiment, it first passes through an electrostatic einzel lens at the output of the source for initial focusing. It then travels through an electrostatic quadrupole triplet before being deflected by a magnetic dipole by 90° into the used beamline. There, the beam is focused into an RFQ accelerator with another quadrupole triplet and an einzel lens, which is the first element shown in Figure 1.1. After the RFQ, a magnetic quadrupole triplet is set up, followed by a dipole magnet for deflection by 45° into the used beamline. Again, the beam can be focused there with a magnetic quadrupole triplet and then reaches the used measurement site where the experiment was set up. These beam optical elements have to be adjusted in order to achieve high particle densities and thus sufficiently high detector currents at the setup of the spectrometer.

Fig. 1.1: Set-up of the beamline in the experimental hall of the 'Institut für Kernphysik'

1.1 ECR ion source

In the experiments performed as part of this thesis, an ECR ion source was used for the generation of highly charged particles. The source itself as well as the setup and optics for beam transport belong to the facilities of the "Institut für Kernphysik" (IKF). It was originally developed as part of an accelerator for materials research using ion beams of different energies in collaboration between the IKF and the IAP [1]. It was later modified and is used in its current configuration to produce a beam of Argon^{8+}-ions with an energy of 120 keV. This charge state is used to achieve the highest possible beam intensities at the experiment, since this charge state has the highest intensities of all states extracted from the source. After approval of the beam time, the experiment was set up at the end of the beamline and the spectrometer was put into operation.

In an ECR (electron cyclotron resonance) ion source, intense ion beams are generated in a two-step process. In the field of two solenoids (see Figure 1.2), electrons are bound to the magnetic field lines
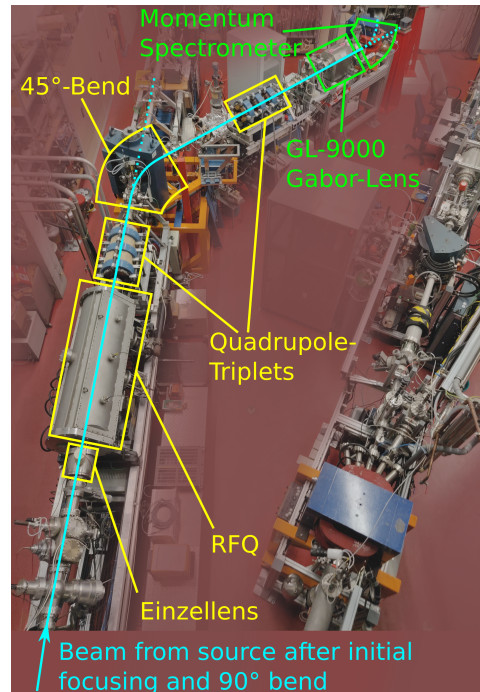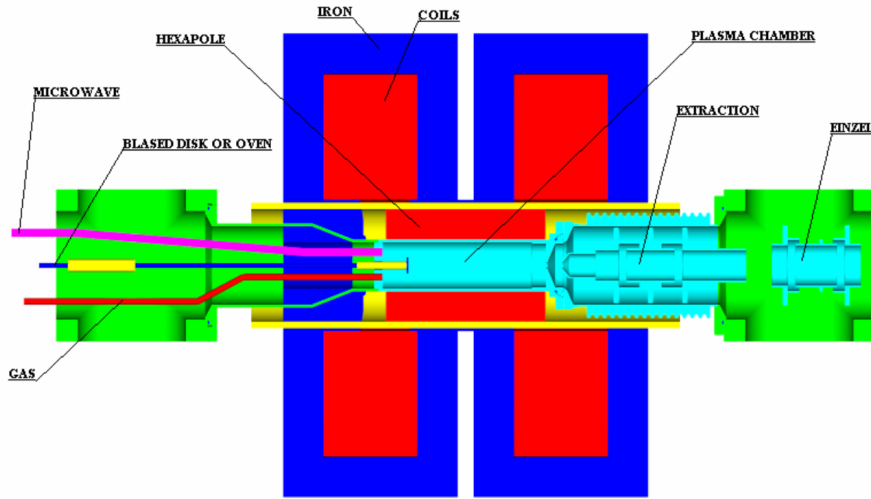
Fig. 1.2: Set-up of an ECR ion source with gas inlet and microwave coupling (left), the plasma chamber with solenoids and sextupole magnets (centre) and the extraction system (right).[2]

due to their low mass. They perform a gyrating motion around the field lines with the so-called cyclotron frequency ω_{Cy}. This results from the mechanics of the circular motion and the Lorentz force in the magnetic field:

$$F_Z = F_L \tag{1.1}$$

$$\frac{mv^2}{r} = qvB \tag{1.2}$$

$$\omega = \frac{v}{r} = \frac{qB}{m} \tag{1.3}$$

With the charge $|q| = e$ and mass $m = m_e$ of the electrons, their cyclotron frequency ω_{Cy} is therefore obtained:

$$\omega_{Cy} = \frac{eB}{m_e} \tag{1.4}$$

The aim is to fulfill the cyclotron resonance condition $\omega_{MW} = \omega_{Cy}$ with injected microwaves of the frequency ω_{MW}. Then energy is transferred to the electrons and accelerates them strongly on their path.

In order to create a large zone within which the resonance condition can be satisfied, the magnetic field geometry is adapted by superimposing a multipole magnetic field (see Figure 1.3). On a closed surface around the centre of the cavity, the resonance condition is then fulfilled at a suitably adjusted microwave frequency, thus strongly accelerating the electrons.
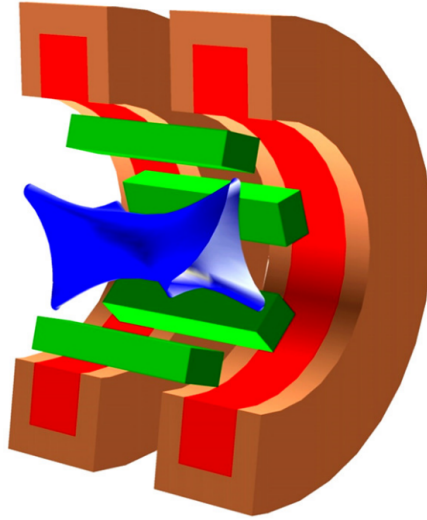
10

Fig. 1.3: Within the superposed magnetic field of the solenoid (red) and the sextupole magnet (green) lies the surface (blue) on which the resonance condition is fulfilled.[3]

As they gyrate around the magnetic field lines, the electrons travel a long path inside the chamber, where they ionize gas atoms with a high probability. These ionisation processes continuously generate new electrons and gas ions. The ions are extremely heavy compared to the electrons and are not accelerated. They are only weakly bound to the magnetic field due to their high mass and remain confined by the space charge potential of the negatively charged electrons. Since the confinement by the electrons is not perfect, a portion of the plasma escapes from the arrangement in the axial direction. Therefore, on one side, through an extractor system in which a high extraction voltage is applied, these ions can be extracted from the source and pre-accelerated into a beam depending on the extraction voltage. Subsequently, the space charge of the ions travelling as a beam is no longer compensated by electrons, causing the beam to expand radially after extraction.

1.2 RFQ accelerator

After extraction from the source, the ion beam drifts through an electrostatic focusing system to an RFQ (radio frequency quadrupole) accelerator for energy variation. This was designed and built as part of the aforementioned accelerator section by A.Schempp [1] as a four-rod structure. In an RFQ a special form of an electric quadrupole is realized. For this purpose, cylindrical electrodes (rods) are mounted in quadrupole arrangement on stems. The mounting is done in such a way that two opposite electrodes are alternately connected to one stem at regular intervals. The individual areas (cells) between the holders each form electrical resonant circuits, since they have an inductance (arrangement of stems, electrodes and mounting plate) and a capacity (between the electrodes) (see Figure 1.4).
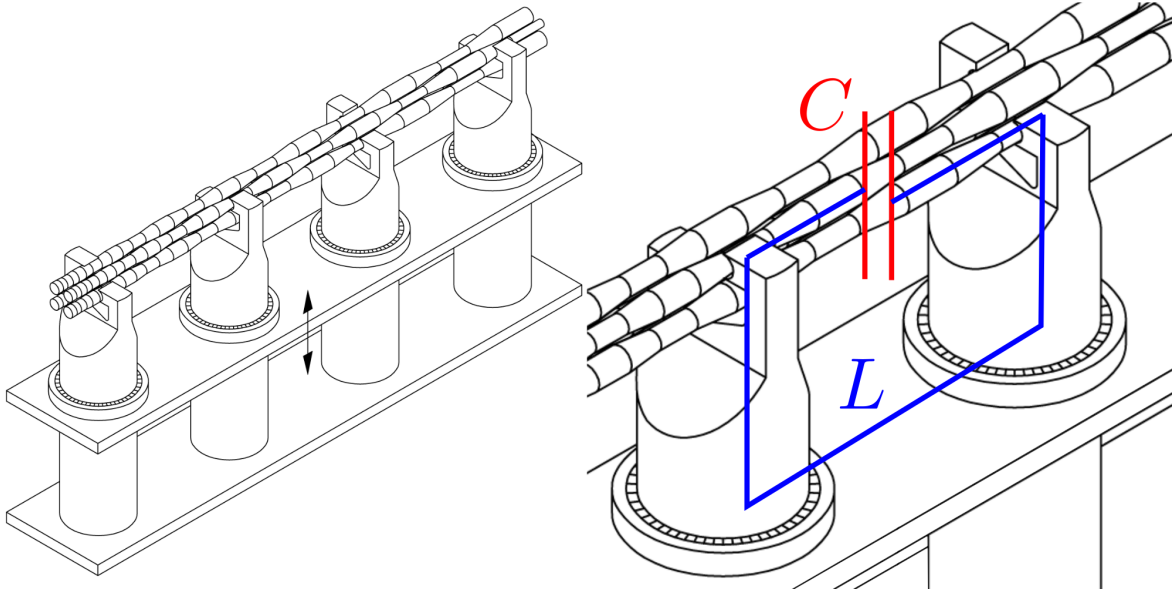
Fig. 1.4: Construction of a four-rod RFQ accelerator with variable energy. The resonant circuit for one cell is shown schematically on the right. [1]

A high-frequency electromagnetic wave with the excitation frequency of the cells natural oscillation is then applied within a chamber by means of a conductor loop. The electrodes are constantly reversed in polarity by the stimulated oscillation which causes the electrodes of the two orthogonal orientations to always have opposite potentials.

Due to the resulting continuously reversing polarity of the quadrupole electric field, charged particles in the electric field are focused in both directions and thus are radially confined. The influence of electric fields for focusing or confinement of ions is particularly large when the residence time of the particles in the quadrupole is high. Therefore, the electric quadrupole is suitable for the transport of especially low-energy ion beams, e.g. directly after an ion source.

Furthermore, in an RFQ accelerator, acceleration of the injected ions is achieved by the geometrical design of the quadrupole electrodes. The electrodes are shaped with a sinusoidal modulation. As a result, the electric fields, which always satisfy the condition $E_{||} = 0$, have not only radial but also axial components (see Figure 1.5). The wavelength of this modulation is chosen in such a way that a certain part of the axially propagating ions is always exposed to an electric field whose axial component points in the direction of movement of the ions, i.e. has an accelerating effect. In order to fulfil this criterion not only in one place, the modulation wavelength must therefore increase with the acceleration of the beam:

$$\lambda_{mod} = \beta \lambda_{RF} \tag{1.5}$$

All ions that are not located within the accelerated region are subject to a negative acceleration due to field components pointing opposite to the direction of motion. As a result, they are decelerated until they are again in the correct phase position to match with an accelerating field. This leads to a decomposition of the beam into individual bunches, which are compressed and accelerated at the same time.

If different final energies are to be achieved during acceleration, the supplied frequency and the resonance frequency of the individual cells must be varied. For this purpose, a movable plate electrically connected to the supports can be used, since its displacement changes the inductance of the individual
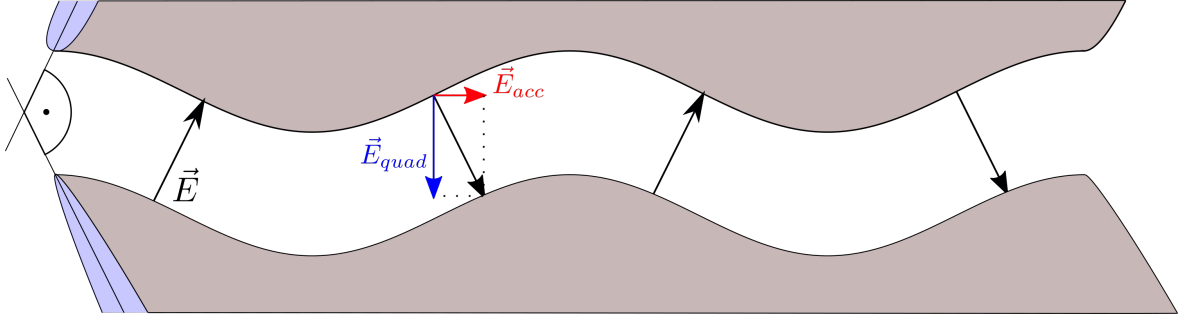
Fig. 1.5: Schematic representation of the electric field between two differently polarised electrodes in the RFQ. It can be seen that there is always a quadrupole component (E_{quad}) and an accelerating component (E_{acc}) of the electric field.

cell (see Figure 1.4).

In the beamline used, the RFQ is operated at a frequency of $85 - 110MHz$ to accelerate the ions to energies of $100 - 200keV/u$. In the experiments with the spectrometer, the RFQ was used as a transport channel for the low energy ion beam. For this purpose, it was operated in the so-called transport mode. To do this, a power much smaller than required for acceleration is applied, resulting in smaller field strengths between the poles. The particles, which only slightly change their velocity, are not in the right phase for acceleration. Thus, they encounter only statistical variations of the longitudinal field, which is why they do not experience effective acceleration. Nevertheless, the confining effect of the alternating quadrupole field can be used for beam transport without acceleration.

1.3 Quadrupole focusing

After the RFQ, the beam is focused with a quadrupole triplet. This arrangement consists of three quadrupole magnets, whose field strengths can be adjusted independently of each other. A magnetic quadrupole is made up of four hyperbolic magnetic pole pieces, with the north and north poles and the south and south poles facing each other in the overall arrangement. This results in a magnetic quadrupole field (see Figure 1.6 (left)). Along the x- and y-direction, the field strength is a normal vector to the coordinate plane and increases linearly with the distance to the beam axis. Thus the field gradient $g = \frac{d\vec{B}_y}{dx} = \frac{d\vec{B}_x}{dy}$ is constant. Therefore, the Lorentz force (see Figure 1.6 (right)) and consequently the radius of the deflection of the particle path is linearly dependent on the distance of the particle to the centre of the quadrupole and accordingly to the beam axis. The direction of the field and the Lorentz force is chosen in such a way that this deflection of the ions in one coordinate direction leads to a focusing effect analogous to a convex optical lens. In the other coordinate direction, the field direction is reversed, resulting in a defocusing effect in this plane. The focal length of a quadrupole of length L in the focusing direction is [4]:

$$f = \frac{1}{\sqrt{k}sin(\sqrt{k}L)} \tag{1.6}$$
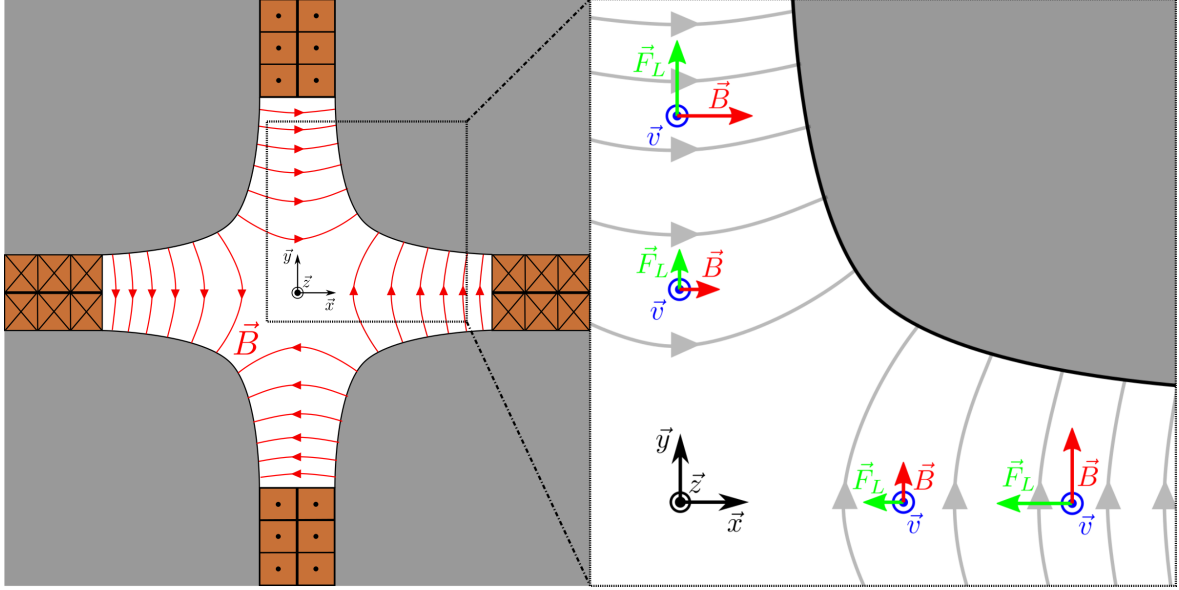
$$\tag{1.7}$$

13

Fig. 1.6: The field of a quadrupole magnet (left), and the Lorentz forces acting on an ion (positively charged, moving perpendicular to the drawing plane towards the viewer) depending on its location in the field(right).

And for the defocusing direction:

$$f = -\frac{1}{\sqrt{k}\,sinh(\sqrt{k}L)} \tag{1.8}$$

$$\text{mit: } k = \left|\frac{q}{p}g\right| = \left|\frac{1}{B\rho}\right|$$

Here q is the charge of a particle, p its momentum and $B\rho$ the magnetic rigidity.

Only in an arrangement of at least two quadrupoles of opposite polarity can an overall focusing effect be achieved, since the beam particles lying in the defocusing plane of the first quadrupole enter the second quadrupole further away from the beam axis, where the field strength and thus the focusing effect is greater. In the focusing plane of the first quadrupole on the other hand, beam particles are brought closer to the beam axis, whereby the defocusing influence of the second quadrupole is weaker. If one assumes the quadrupoles to be approximately thin lenses, the total focal length of two quadrupoles with a distance s results:

$$\frac{1}{f} = \frac{1}{f_1} + \frac{1}{f_2} - \frac{s}{f_1 f_2} \tag{1.9}$$

1.4 Bending magnet

Subsequently, the beam is deflected to a 45° angle to reach the used experimental area. A bending magnet is used for this purpose. It consists of a magnetic dipole built from two field coils wound around an iron yoke. The magnetic field lines are guided inside the yoke due to the high permeability of the iron. They emerge at the pole shoes and form an approximately homogeneous magnetic field within the gap. Within this magnetic field, the ions are forced onto a circular trajectory. The radius of this path can be adjusted with the magnetic field strength. The geometry of the field is chosen in such a way that, if the radius is set correctly, the ions exit the field at a certain angle with respect

to the original beam direction (45° for the used beam transport line). In addition, a dipole of this design leads to geometric focusing, since ions entering the field further out have a longer path in the field, while those entering further in have a shorter one (see Figure 1.7).
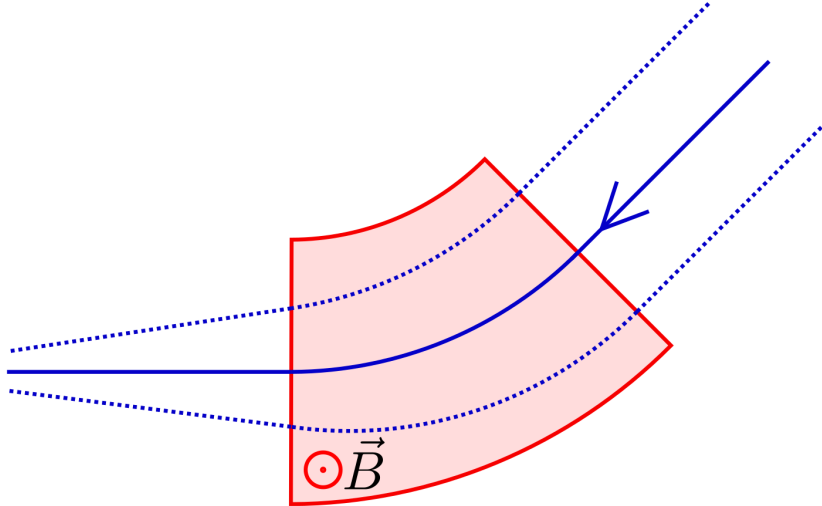

Fig. 1.7: Illustration of the deflection of a (positive) ion beam in the dipole field: Ions on the nominal path are deflected by a fixed angle. Ions that enter the dipole field further outside are deflected along a path with the same bending radius, but which is longer due to the geometry of the field. As a result, their deflection angle is larger. Ions that enter further in have a shorter path in the field and are deflected by a smaller angle. This leads to a focusing effect (geometric or weak focusing).

1.5 Gabor lens

1.5.1 Working principle

A gabor lens is an electron trap which produces a plasma through ionization processes and confines the electrons with a configuration of a longitudinal electrical field and a parallel magnetic field. The electric field is generated between two ring electrodes at the ends and the main cavity itself in the center. When polarity is set to positive potential on the cavity and negative potential on the outer electrodes, electrons are therefore longitudinally confined. To prevent them from rapidly accelerating radially and hitting the center electrode, an axial magnetic field is generated by a solenoid. Electrons that are accelerated in the electric field thereby have a momentum and are thus influenced by the magnetic field. Due to their low magnetic rigidity, they are bound to the magnetic field and gyrate around the magnetic field lines. Superposed with the electrical force directed longitudinally inwards, this leads to a spiral movement around the magnetic field lines and an oscillating movement in the longitudinal direction. Initially, electrons can be produced by various possible ionisation processes, e.g. by cosmic radiation (photo-ionisation). These electrons are not lost in this particular field configuration, but gain kinetic energy during their movement in the electric field, depending on their initial location. Through collisions with residual gas atoms, they produce further pairs of electrons and positively charged ions. While the ions are accelerated outwards in the electric field and thus quickly leave the lens, the electrons remain inside and "fill" the lens through further ionisation processes. This process
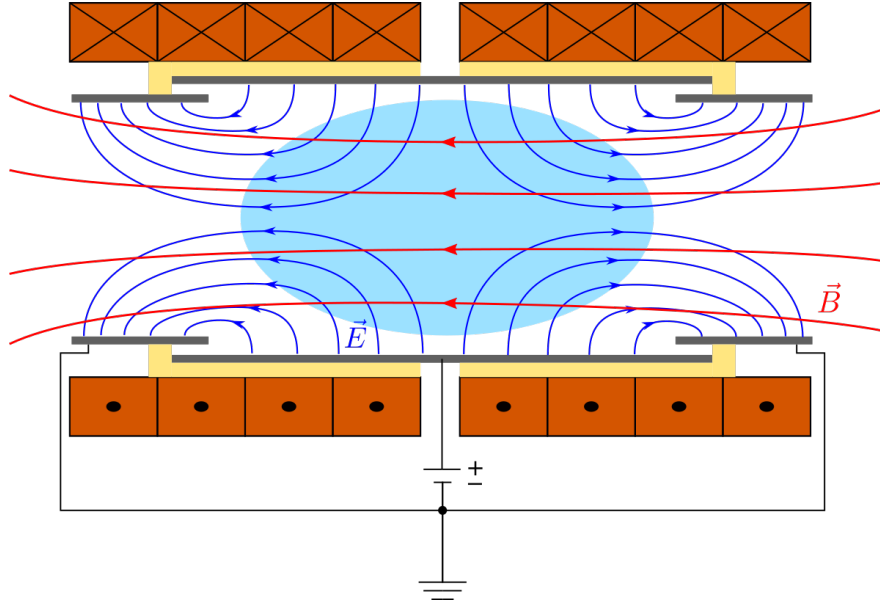
Fig. 1.8: Overview of the Gabor-Lens setup with the electric field generated by the high voltage between anode and cathode (blue), the magnetic field generated by the solenoid around the cavity (red) and electron cloud (light blue)

can continue until the intrinsic field of the trapped electrons becomes so strong that the potential difference between the centre of the lens and the cathode rings becomes too small, causing electrons to be lost longitudinally. Similarly, electrons can be lost at the walls when they hit the anode on their gyrating path. Both the electric and magnetic field can be limiting factors for the maximum confined electron density. Ideally, they are adjusted so that the theoretical density limits of each are the same. The relationship between the two field strengths at which this condition is met is called the operation function. The ratio of the actual electron density to the theoretical maximum density at given field strengths is called the filling degree.

1.5.2 Space charge compensation und focusing

The structure of the Gabor lens, when it is not filled with electrons, also has beam-optical properties depending on the fields. On the one hand, the magnetic field of the solenoid has a weak focusing effect due to the effects of the beam ions entering and leaving the field. On the other hand, the structure of the electric field is that of an electrostatic einzel lens. In this lens, an ion beam is focused by the radial components of the electric field. Both effects must be taken into account when observing the influence of the electron cloud on ion beams. The influence of the electric field on the ion beam, however, decreases with increasing filling ratio of the gabor lens, because the potential inside the lens becomes equal to the cathode potential. The electron cloud itself has an influence on an ion beam moving logitudinally through the lens in two different ways. Firstly, the existing negative space charge of the electron cloud compensates for the positive space charge of the ion beam. If the density of the electrons is approximately equal to the density of the beam ions, the potential of the beam is neutralised. This has two beneficial effects for the beam transport: Especially in the LEBT (low-energy-beam-transport) section of accelerators, the space-charge forces of the ion beam play an important role, since they lead to a permanent widening of the beam, which must be compensated by focusing elements. Especially at low energies, magnetic focusing elements are less effective because their focusing strength depends

on the momentum of the particles. If, however, the ion beam is transported without space charge, there is no expansion. Due to the simple construction of the Gabor lens, it is easily scalable and can theoretically also be used on a large scale for space charge compensation in beam transport channels. The second effect is the focusing of the beam by the eigen fields of the electron cloud. Assuming a homogeneous charge distribution of the electrons in the lens, the electric field inside the cloud is linearly dependent on the radius. Thus, there is an inward radial force acting on positive ions moving through the lens, which increases linearly with the distance to the axis. This property leads to a focusing of the beam with linear optics.

Assuming a thin lens, the focal length of the Gabor lens can be determined as:

$$f = \frac{\epsilon_0}{n_e e L} \frac{1}{q} \frac{p^2}{2m} = \frac{\epsilon_0}{n_e e L} \frac{E_{kin}}{q} \tag{1.10}$$

where n_e is the confined electron density, L the length of the lens and p, q and m or E_{kin} the properties of beam particles to be focused.

1.5.3 Research

Spectrum of emitted Ions

Various properties of the Gabor lens can be measured with the measuring station set up as part of this work. On the one hand, the ions accelerated out of the Gabor lens, which are produced by ionisation of the residual gas, can be examined in the momentum spectrometer. The momentum of these ions or their kinetic energy depends on various variables. The energy gained by an ion during acceleration in the electric field of the lens correlates directly to its spatial origin. If an ion is created in the centre of the lens, it can pass through the full potential difference between anode and cathode. If, on the other hand, it is generated near the cathodes, the kinetic energy gained until it leaves the field is much lower. By observing the momentum or energy distribution of the ions, conclusions can therefore be drawn about the spatial distribution of the ionisation processes inside the lens. If the lens is in a state of equilibrium, i.e. filled with electrons, the potential seen by the ions in the centre of the lens decreases due to the negative potential of the electron cloud. They can then reach a maximum energy that no longer corresponds to the potential difference of the electrodes, but is lower, depending on how strongly the anode potential is compensated. Therefore from the upper limit of the energy distribution of the ions the potential of the electron cloud and thus the density of the electrons or the degree of filling of the lens can be deduced.

Charge changes in beam ions due to ion-electron-interaction

The purpose of using Gabor lenses in beam optics of accelerators is mainly for space charge compensation of high intensity heavy ion beams. Therefore the effects of the confined electron cloud on beam ions need to be investigated. Since the ions pass through a relatively static electron cloud during operation of the Gabor lens, it is obvious that beam ions may interact directly with the electrons. In this process, they can be subjected to change of charge either by electron capture or by impact ionisation, so that their charge increases or decreases. The interaction cross-section for both processes depends on the relative velocity of the electrons and the ions. At high relative velocities, as is the case with an accelerated ion beam, these charge change effects within the lens should be very small. In order to investigate the charge transfer processes in the beamline, the momentum distribution of the beam is measured with the Gabor lens switched off. Subsequently, the same measurement can be carried out with the Gabor lens switched on in order to visualise any change in the rate of charge changes.

For these investigations and further research the Gabor-Lens "GL-9000" is used, which was built for GSI/FAIR as part of the project "Development of a compact LEBT section for high-intensity heavy ion beams". With the current setup it can be driven with a range of electric and magnetic field configurations which lead to different states of the confined electron plasma cloud. The control of the gabor lens via a remote control and measurement system was done by Dönges[5]. Also in the future further investigation on the correlation between field strengths and the state of the cloud is planned.

Chapter 2

Momentum spectrometry

In order to investigate the momentum of charged particles, their deflection in a magnetic field is observed. For this purpose, a magnetic field is generated that is as homogeneous as possible and has a known strength and extent. The particle path runs through this magnetic field. There, the particles are deflected along circular paths until they leave the magnetic field. The radius depends on the particle momentum as well as their charge and mass. Knowing that radius and the strength of the magnetic field, the magnetic rigidity and thus the momentum of the particle can be calculated. Also, if the mass of the particle is well-known the particle momentum can be transformed to find the magnitude of velocity or its kinetic energy. Otherwise, if the kinetic energy is well-defined due to the method of acceleration, the mass of the particles and thus their species can be investigated. In this use case the presence of beam particles under a certain, well-defined deflection angle from the undeflected straight beam direction is measured dependent of the magnetic field strength. The magnetic field strength B depends on the current run through the dipole magnet and is calculated from the measured current and known calibration data. The required radius ρ of the circular trajectory that aims a particle directly at an aperture in front of the measuring device is a physical property of the spectrometer chamber inside the dipole magnet. From this known magnetic rigidity $B\rho = mv/q$ the momentum can be derived as follows:

$$p = mv = B\rho q \tag{2.1}$$

Also the kinetic energy can be calculated:

$$
\begin{aligned}
E_{kin} &= \frac{p^2}{2m} \\
&= \frac{(B\rho q)^2}{2m}
\end{aligned}
\tag{2.2}
$$

Or if the energy is known, the mass of the particle is:

$$m = \frac{(B\rho q)^2}{2E_{kin}} \tag{2.3}$$

If a particle beam or bunches of particles are investigated, usually a spectrum of momenta is observed. In a detector which is placed in the deflected direction, the number of incoming particles can be measured as an intensity of charged particle current. One can map these spectra by changing the magnetic field and plotting the measured intensity in the detector dependent on the particle momentum calculated from the field strength.
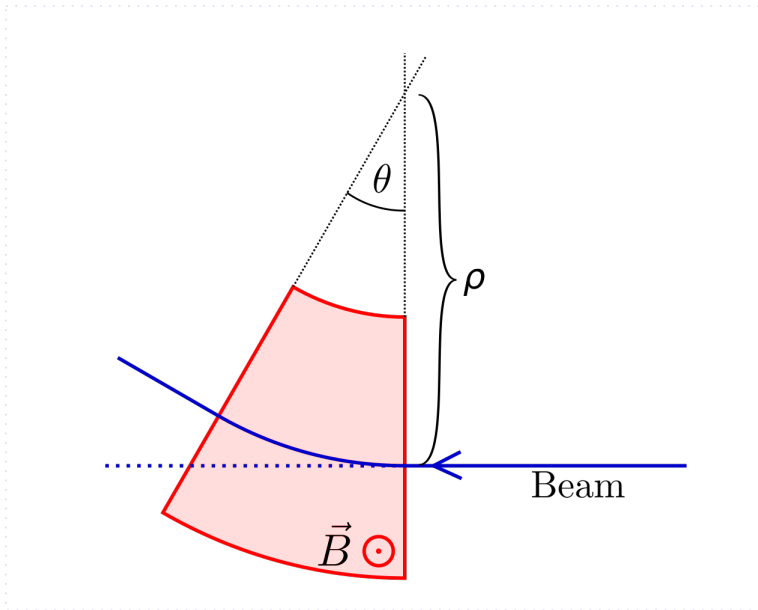
Fig. 2.1: Beam deflection in magnetic field $\vec{B}$ on a circular trajectory with radius ρ. The beam exits the magnetic field under a deflection angle θ.

2.1 Spectrometer structure

For the momentum spectrometer the deflection of particles on a well known trajectory is required. Therefore one needs to know the direction the particles have before entering the deflecting magnetic field (straight direction) and after exiting the field (deflected direction). Both need to be known as precisely as possible as their erros add up when calculating the radius of deflection inside the magnetic field. To determine these directions small circular apertures are used. One is placed in front of the dipole, another one in front of each detector. A magnetic field with known characteristics is needed to ensure the accuracy of the calculated magnetic rigidity of detected particles.

An electromagnetic dipole with an iron yoke is used, which is calibrated with a hall probe prior to measurements. Calibration measurements for the used dipole configuration have been done by Plag[6]. Between the pole pieces of the magnet sits a vacuum tight chamber which contains the three apertures and the detectors.

2.1.1 Faraday cups

Two Faraday cups are used as detectors for the ions arriving behind the apertures. The basic principle of their operation is to neutralise the charged particles on impact by collison or absorption and to let the transferred charge drain to earth via a current measuring device. The measured current is equivalent to the amount of charge that has impinged on the cup per time.

In order to measure the actual ion current as accurately as possible, one must avoid disturbing effects caused by other
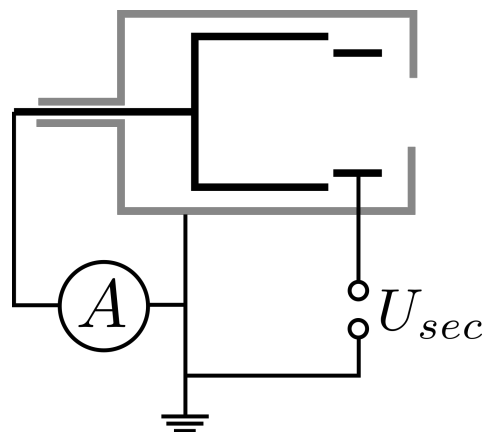

Fig. 2.2: Faraday cup: Diagram of the electrical setup with current measurement and secondary electron suppression
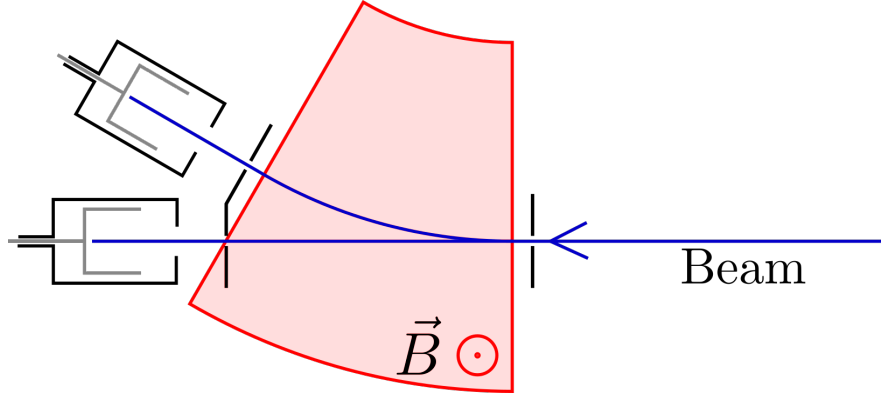
Fig. 2.3: Structure of the measuring arrangement

charge carriers. These are mainly caused by the generation of secondary electrons when ions hit the Faraday cup:

When the ions enter the surface of the detector, they release their kinetic energy to the material. This causes electrons in the surface to overcome the binding energy and escape from the surface. If these are lost afterwards, they affect the measurement of the ion current, since the current of the escaped electrons is added to it (it carries the same sign, since the electrons are oppositely charged and are carried away). To avoid this, a negative potential is applied to a ring in front of the actual Faraday cup, so that all electrons generated inside the cup are redirected into the cup (see Figure 2.2).

2.1.2 Dipole

A dipole magnet with an iron yoke is used to generate the magnetic field. Here it is first assumed that the field is homogeneous and spatially limited to the size of the pole shoes of the iron yoke. The deflection of the ions then depends only on the strength of the magnetic field inside the dipole. This strength is directly proportional to the current through the dipole coils:

$$B = \mu_0 \mu_r \frac{NI}{\mu_r l_{Air} + l_{Yoke}} \tag{2.4}$$

The magnetic field strength in the dipole was determined experimentally by Plag[6]. Using a Hall probe, a calibration curve of the magnetic field was measured as a function of the current. This not only enables a more precise, experimentally confirmed calculation of the strength of the magnetic field, but also provides information about the influence of the hysteresis effect, which is caused by the magnetisation of the iron core in the dipole magnet. To facilitate the determination of the magnetic field strength, all measurements with the spectrometer were always carried out with a temporally increasing magnetic field and after a sufficient time with no excitation current to minimise the remaining magnetisation. In this way, a single calibration curve can be used for the given polarity. A linear function was fitted to the measured values, which shows very good agreement with the measured values. The fit has the greatest error around the zero point, since the field strength must be zero with no current and no magnetisation. Its value $B_0 = 14.2 mT$ is still very low in comparison to the used field strengths for the deflection of even very low energy ions. In addition, the spectrometer is always operated with a current or magnetic field for measurement of momentum that is far away from the zero point, so that this deviation does not affect the calculation of the momentum. It should be noted that when measuring the beam current in a straight direction, one must be aware of the magnetisation or hysteresis effect which are most prominent around the neutral point.
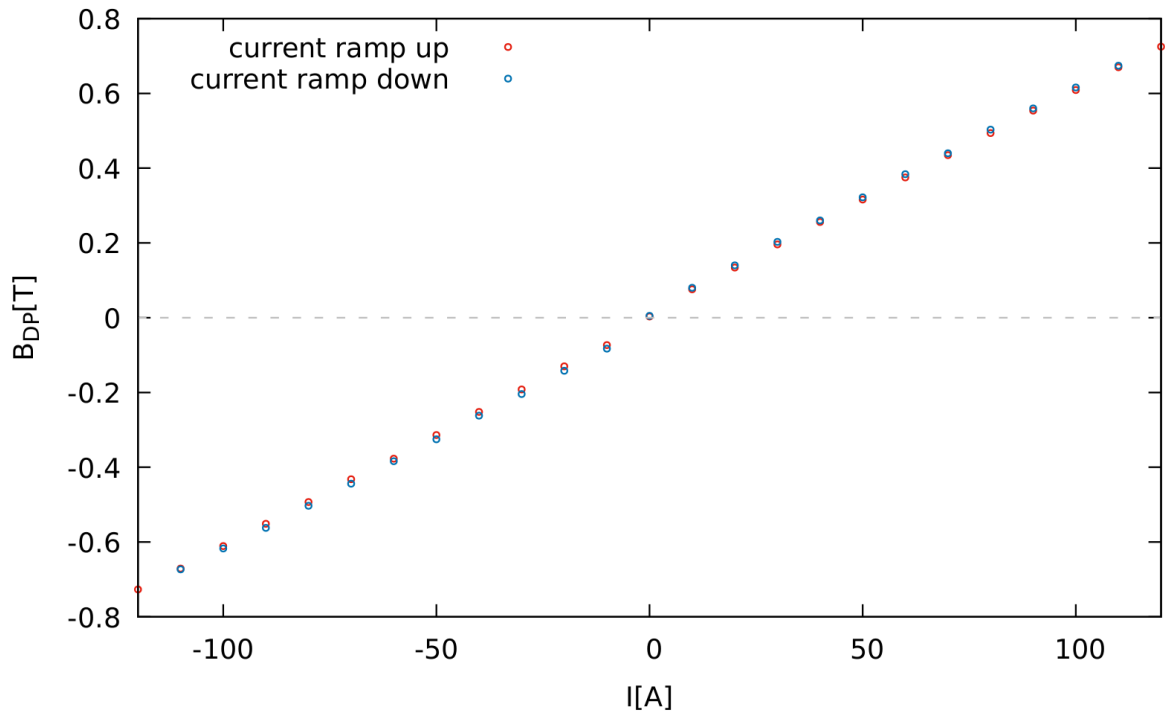
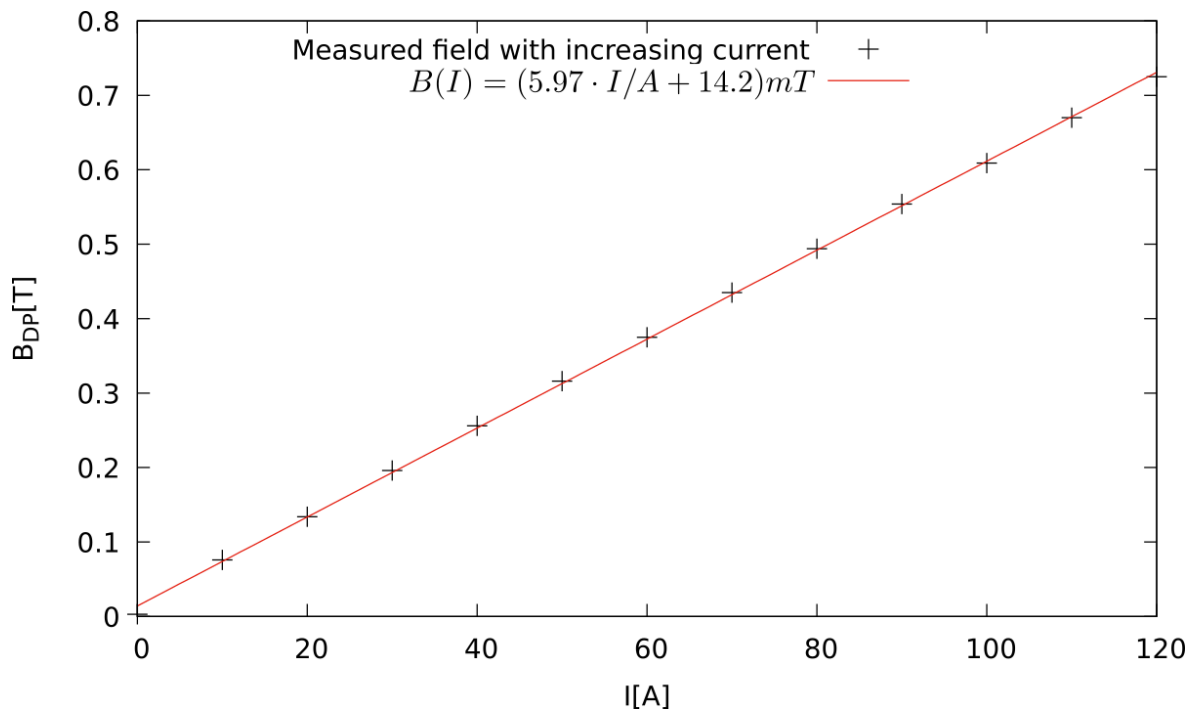**Fig. 2.4:** Calibration data for magnetic field vs. current with hysteresis measured by Plag[6]

Fig. 2.5: Calibration data for positive and increasing current ramp with linear fit $B(I)$

2.2 Measurement and control

The whole setup is designed for operation under conditions found in large accelerator facilities and lab environment. Therefore remote operation was a main goal of the development. A Python 3 backend software was developed that communicates with all devices via a network connection. Furthermore the process of plotting a spectrum requires many measured points with multiple samples at each point. For that reason a software frontend was also implemented that enables automated series of measurements with an arbitrary number of setpoints.

2.2.1 Measurement equipment

Power supply

One of the two main variables that need to be continuously measured in the spectrometer is the magnetic field strength of the dipole magnet. To obtain the wanted setting of the magnetic field the current in the dipole coils is adjusted. A high precision, high current power supply is used for this purpose. On the one hand it delivers high enough currents to investigate higher energy particles. On the other hand it provides remote operation capabilities as well as high precicsion internal current measurement. To determine the needed dipole current for a given species of particle with given momentum or kinetic energy, equations (2.1) and (2.2) can be modified to get:

$$B = \frac{p}{\rho q} = \frac{\sqrt{2mE_{kin}}}{\rho q} \tag{2.5}$$

With the known radius ($\rho = 0.44m$) of the deflected trajectory and the field vs. current calibration curve of the dipole ($B = (5.97 \cdot I/A + 14.2)mT$) one obtains:

$$I = k\frac{p}{q} - I_0 = k\frac{\sqrt{2mE_{kin}}}{q} - I_0 \quad \text{with: } k = 381\frac{A}{Tm} \quad \text{and: } I_0 = 2.38A \tag{2.6}$$

The power supply was chosen to have a maximum current delivery of $120A$ at a maximum power of $4.2kW$. It is able to measure current and voltage internally and provide the measured values via an interface. The dipole magnet itself is rated for a maximum current of $62A$ with watercooling which didn't need to be implemented yet.

Detector current measurement

The other measurand in the spectrometer is the current of charged particles impinging in the Faraday cup. It is very small and is measured with a highly sensitive picoamperemeter (Keithley 6482). It achieves an accuracy of $1.00\%+2pA$ when measuring the current in the used $2nA$ range. It is possible to use a double-shielded cable ("triax") to ensure the lowest possible interference from outside. However, as these cables are relatively expensive and their advantages for this setup are not clear, a common coaxial cable was used for the first tests. It was found that the measured value of the current is subject to fluctuations in the range of about $\pm 6 * 10^{-12}A$ and thus some small peaks in the mass or energy distribution, especially of the ions from the Gabor lens, are indicated in this noise but are no longer significant. The work of Krause[7] was consulted to investigate the use of coaxial cables in lowest-current applications. Several effects play a role and have a varying impact on the measured value of the current: Piezoelectric effects generate a low voltage when the cable or rather the insulation layer between the inner and outer conductor is mechanically deformed, which leads to measurable current signals due to the very low input resistances in low-current measurement. In the triboelectric effect, charge carriers are separated by the friction of the insulator with the conductors, especially at the large

23

Material	Volumen- widerstand $\Omega\,\mathrm{cm}$	Oberflächen- widerstand Ω	Piezo- elektrischer Effekt	Tribo- elektrischer Effekt	Dielektrische Absorption
Saphir	$> 10^{18}$	-	wenig	mittel	wenig
PTFE	$> 10^{18}$	$> 10^{18}$	stark	stark	wenig
Polyethylen	$10^{15}-10^{18}$	10^{13}	wenig	mittel	wenig
PVC	$5 \cdot 10^{13}$	-	mittel	mittel	stark

Tab. 2.1: Comparison of different isolator materials' properties [7]

contact surface with the outer conductor, which then drain through the cable as measurable current. Furthermore, charge carriers can also be separated by dielectric absorption. There they are absorbed or released by the insulator over a longer period of time. According to the investigations of Krause[7], it turns out that especially polyethylene (PE) as an insulator material has a consistently acceptable susceptibility for all these effects. However, in order to also minimise the triboelectric effect, which cannot be completely ruled out for any of the tested materials, a cable was selected that not only uses PE as the insulator material, but also has a small cross-section. This minimises the contact area between the outer conductor and the insulator, which means that less surface area is available for charge separation.

Furthermore, due to the smaller diameter compared to a thicker cable, a smaller displacement of the conductor layers against each other is achieved with the same deformation, which should also reduce the effect. After using cables with these properties, a fluctuation of the quiescent current measured value by a maximum of one significant digit in the display of the picoamperemeter or by approximately $\pm 7 \cdot 10^{-14} A$ in the digital readout can be achieved despite the fact that the sensing cable is not double-shielded. This inaccuracy is less than the noise due to charge carriers generated randomly within the set-up, which hit the Faraday cup during the measurement but do not originate from a defined source.
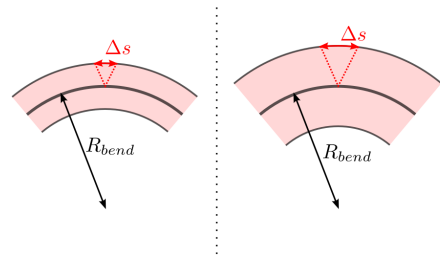

Fig. 2.6: Displacement between insulator and outer conductor during deformation of thin and thick coaxial cable

2.2.2 Network setup

In order to make the entire measuring station remote controllable, a sufficiently fast data connection from outside is necessary. It is required to transmit all commands for controlling the devices and their return values via a common interface. To achieve this, the control of the devices was realized inside a local network, which is then made accessible from outside via a router. For this purpose, the high-current power supply already has an Ethernet interface, but the picoamperemeter communicates via a serial interface. It is therefore connected to an Ethernet serial gateway, which enables the connection to the network. Last but not least, the security of the data connection must also be ensured. Therefore, all devices are located in a local area network (LAN), in which all network devices cannot be reached from the outside. The computer required for control is also located within this network. The central control software, which also contains all the command sets for controlling the devices, runs on this computer. Only this computer can be connected to from outside the local network (from another network or from the Internet) by port forwarding through the router. This can fall back on the
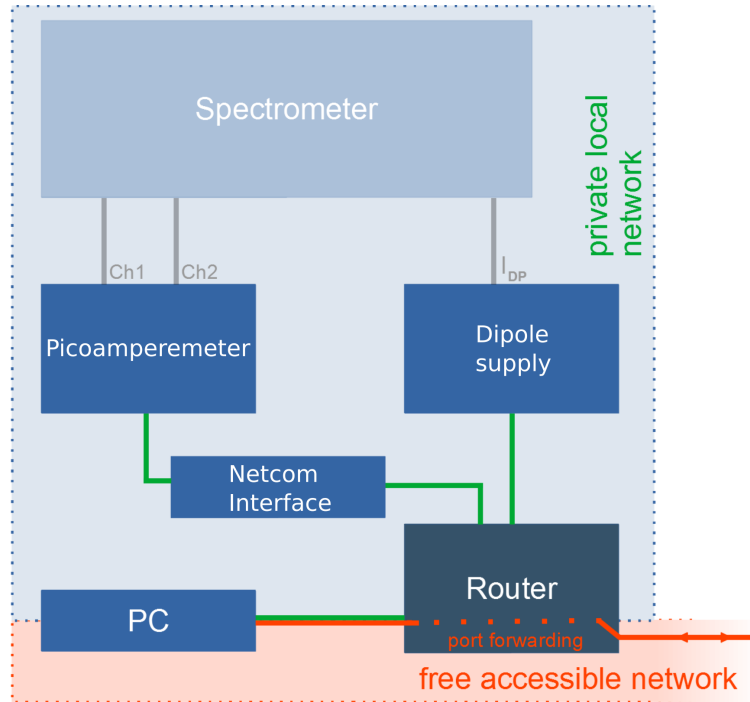
Fig. 2.7: Network setup with all used devices

existing, secure SSH protocol and can thus be secured either with a simple password protection or via security certificates. Furthermore, the graphical user interface of a program can also be transferred via this SSH connection. By using this function, the entire control software with the graphical user interface can run centrally on the computer located inside the measurement rack. It is then possible to control the measuring station with any device that is connected to the external network and supports SSH, provided that it is authorized by password or certificate, without the need for installation. The physical connection to an external network is made with a fiber optic cable. The usual connection via (copper) Ethernet cable inside the terminal is thus galvanically isolated from all devices and interfaces located on the outside. This allows the whole setup (measuring rack with computer, dipole magnet and detector chamber) to be brought to any potential with respect to ground, e.g. to generate an decelrating field, while control from outside is possible simply by connecting to a fibre optic network or, after using a converter, to an RJ-45 interface.

2.2.3 Software for control and automated measurement

For the control of the devices and for the readout of measured values a software was developed, which allows to make the necessary settings, to control the power supply of the spectrometer and to read out measured values from the picoamperemeter. In addition, a single automated measurement series comsisting of several set points for the dipole current can be run as well as a whole set of measurement series, which are then automatically processed one after the other. The software has a graphical user interface, which is used to enter the parameters of the desired measurement series. Besides that, the current measurement data is graphically displayed here in real time. A file with all recorded measurement values is automatically created for each measurement series. Likewise in a time interval of $0.5s$ all relevant parameters are deposited in a log file, which is again generated with each program start. Due to the network structure described above, the control software is a central program, which

is divided into frontend (user interface, graphical display and data output) and backend (network connection, command sets, control and readout as well as automation routines).

Backend

In the backend, the connection to the devices is first established via TCP sockets each time the program is started. The syntax of all commands required to control the individual devices is stored as a dictionary. The individual commands, which are then sent as a string to the respective device, are generated dynamically with the associated set value in each call. In the case of the power supply, this involves setting the voltage, the current and the ramps for both. Additionally, the return of a current or voltage measurement value is triggered by a command. For the picoamperemeter, the current measurement values of the two channels are requested and settings for the sample rate are made. All responses that then come back from the devices are received and recognized as either a confirmation response or a specific measured value. A complete set of all last known measured values is constantly available in the program flow and is used e.g. to write the output files in another routine or to enable graphical output in the frontend. The routines that perform these send- and receive-functions run in theri own threads independently of each other and of the rest of the program flow. All commands passed to the send routine are stored in a queue and transmitted to the respective device one after the other in a time interval necessary for processing. All returned values are read out from the buffer of the TCP socket by the receive routine at regular time intervals and broken down into the individual strings, from which the measured values are then taken.

The routine for the automated measurement is started as soon as it is requested by the frontend. It is given all parameters that are necessary to run the set points. It then runs independently of the rest of the program flow in its own thread until the measurement series (or the collection of measurement series) is completed or terminated by user input in the frontend. In time intervals given by the user it passes target values to the send routine, waits until the power supply reaches these values and then stores an adjustable number of all measured values in quick succession. In the file for recording a series of measurements, each set of measured values is written as a new line. After that it moves to the next point. At the end of all measurement series or if the user cancels the measurement run, it outputs new set values that are valid until the next start of a measurement. In addition, over the entire runtime, as part of the main loop of the main program, all possible measured values are written to the log file at regular intervals with an associated time stamp.

Frontend

In the frontend, operation by the user is enabled, and the recorded measurement data is processed and displayed graphically. A graphical user interface is used for this purpose. The main functions are starting and stopping a measurement series and entering the necessary parameters (start and end values for the dipole current, current increment per measurement step, the step and measurement time and the maximum voltage). Beyond that, a collection of measurement series can be created in the set window, which are then run one after the other.
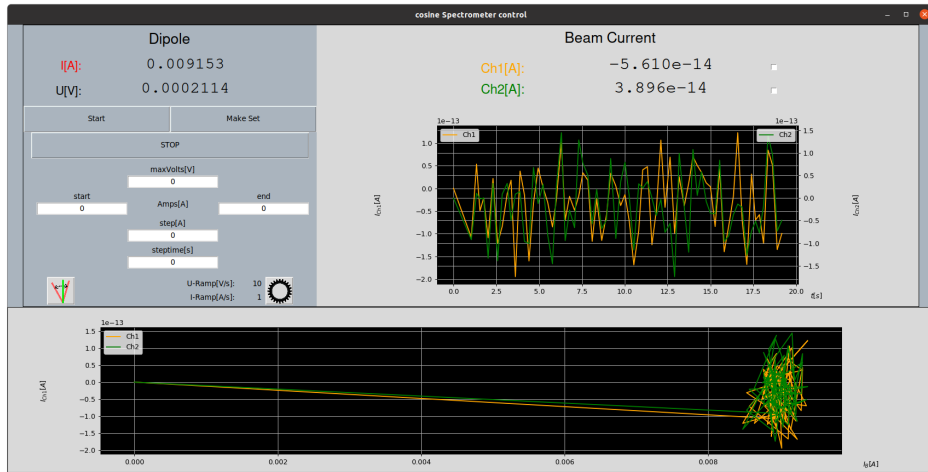
Fig. 2.8: Screenshot of the graphical user interface of the control software. One can see the input mask and controls for a current measurement series, the current measured values of both the power supply unit and the picoamperemeter as well as live plots of the two channels of the picoamperemeter, which are plotted against time (top) and against the measured current of the power supply unit (bottom).
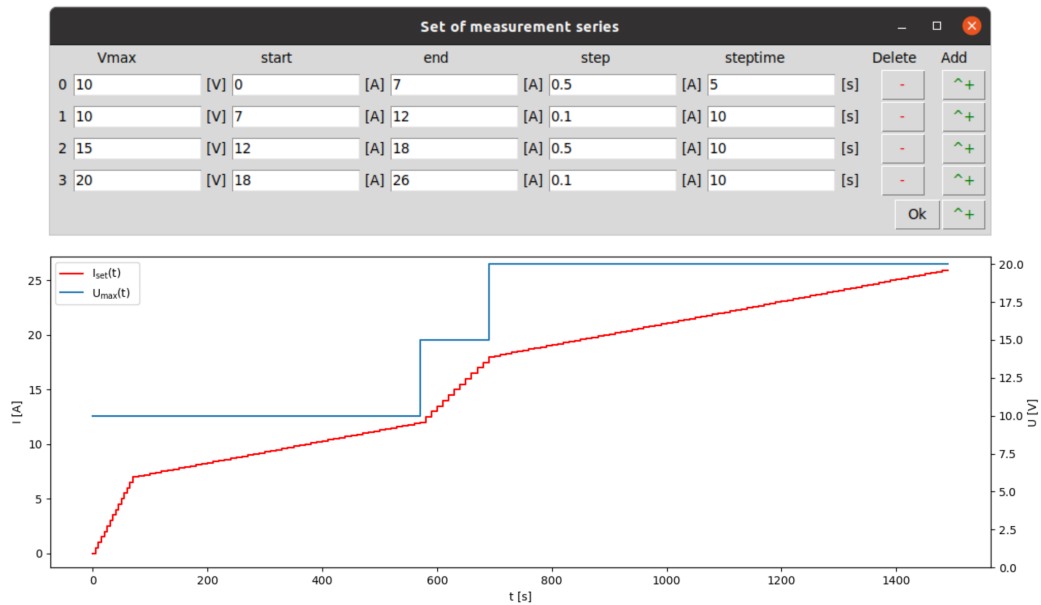

Fig. 2.9: Screenshot of the set window in which several measurement series can be preconfigured (top) as well as the curves for current and voltage of the power supply resulting from the inputs. The differently set steps for coarser and finer scanning of a current range can be seen.

For setting the position of the spectrometer, the user interface contains a setting tool which displays the intensity of the ions impinging in the straight direction as an automatically scaling bar graph in real time.

For visualisation of measurements two plots are updated in real time to display the measurement

data. One plot shows the currents measured in the two detectors since the start of the program as a function of time and thus provides an overview of several successive measurements in comparison as well as the events outside the measurement periods. The other plot is created anew each time a series of measurements is started. Here the current in the two detectors is plotted as a function of the dipole current. It provides a more accurate representation of the measurement currently in progress or completed and allows initial conclusions to be drawn from the results, e.g. to scan a smaller range of interest with a higher resolution. The two plots are animated in separate threads so that they are updated at fixed time intervals independently of the main loop of the main program.

Chapter 3

Experiments and Observations

3.1 Spectrometry of low-energy charged particle beam

In the ion source, highly charged Argon ions with different charge states are generated and extracted with an extraction voltage of $15kV$. For the experiments with the spectrometer the most produced charge state Ar^{8+} is selected, so that the ions have a kinetic energy of $120keV$ after extraction. The RFQ accelerator has been operated in transport mode, as described, so that the ions do not undergo any further acceleration until they are deflected in the dipole and detected as a continuous beam with a certain energy or momentum distribution in the faraday-cup. This distribution is measured with the spectrometer for different settings of the beamline and with regard to the beam energy distribution $I(W)$ as well as the occurrence of charge changes.

3.1.1 Beamline setting

In order to transport the ion beam through the RFQ and then deflect it under the correct angle into the 45°-beamline, the settings of the RFQ power and the 45°-dipole were first roughly adjusted and then fine-tuned with the aid of the spectrometer. Here, the parameters were adjusted until the distribution in the spectrometer was as close as possible to the target energy (energy of the beam from the source, $E = 120keV$) and had the smallest possible width ΔE_{FWHM}. Then it can be assumed that the transport in the RFQ takes place with insignificant distortion of the energy distribution of the ion beam and the adjustment of the 45°-dipole deflects the beam centrally onto the aperture of the spectrometer. Figure 3.1 shows examples of some distributions at different RFQ power settings.
A width of the energy distribution of $\Delta E_{FWHM} = 5.32keV$ was achieved by setting the RFQ, or a relative width of: $\frac{\Delta E_{FWHM}}{E} = 4.4\%$
Figure 3.2 also shows some distributions, here for different current settings of the 45°-dipole. After adjusting the 45°-dipole, the spectrometer was finely aligned to the beam axis so that the center of the distribution in the non deflected case lies exactly in the straight channel of the spectrometer.
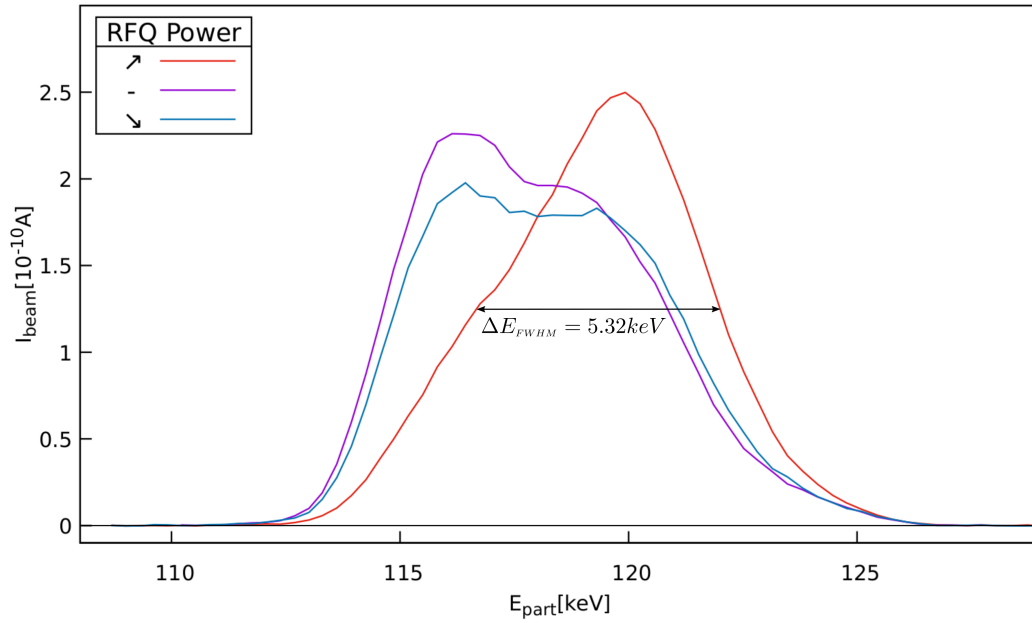
Fig. 3.1: Energy distribution of the beam ions depending on the RF power in the RFQ. At the correct power for unaccelerated transport, the energy distribution of the ions is centered around the target energy of $120keV$ gained from the extraction, so there is neither deceleration nor acceleration.
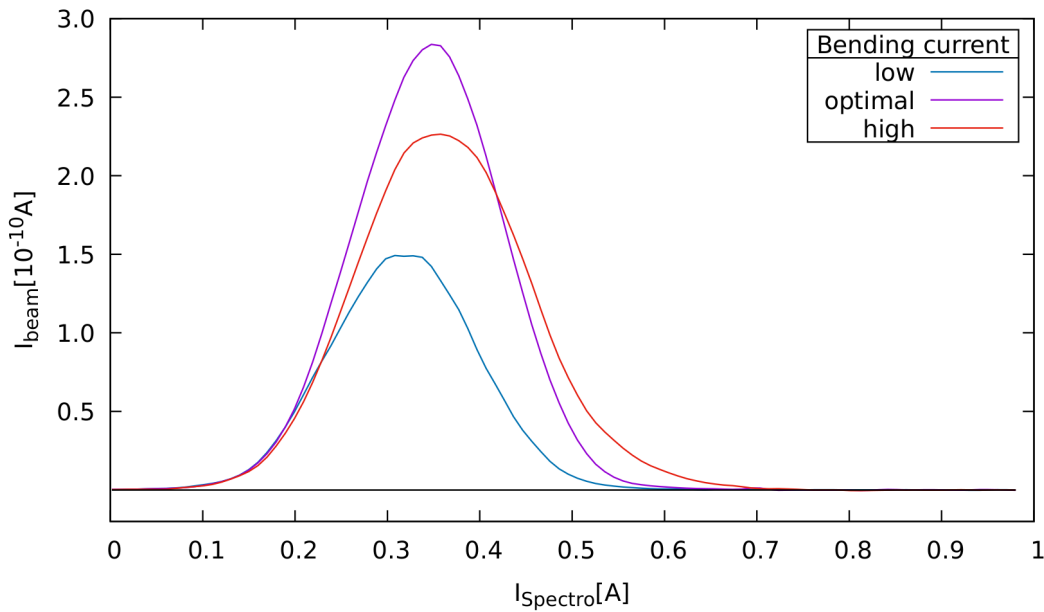

Fig. 3.2: Distribution of the beam ions depending on the setting of the 45°-dipole. When this distribution was recorded, the spectrometer was not yet finely aligned to the beam axis, so the beam shows up as a distribution under very small excitation currents in the straight channel. The optimal setting of the bending dipole is reached at the highest intensity, since the center of the beam then lies in the aperture of the spectrometer.

3.1.2 Observed particles and energy

As described earlier, Argon^{8+}-ions are generated in the ion source and extracted with an accelerating voltage of $15kV$. First, a spectrum of the Argon^{8+}-beam was measured. A control measurement was made after the source was turned off and reignited, to ensure the beam properties remain constant over multiple measurements. These two measurements are shown in Figure 3.3. For Argon ions, mass number 40, with charge 8, the equation for the energy can be derived from equation 2.6:

$$E_{kin} = \frac{1}{2m} \left[\frac{q\,(I + I_0)}{k} \right]^2 \tag{3.1}$$

$$\text{or simplified:} \quad E_{kin} = \epsilon (I + I_0)^2 \tag{3.2}$$

$$\text{with: } \epsilon = 8.53 \cdot 10^{-17} \frac{J}{A^2} = 0.532 \frac{keV}{A^2} \quad \text{and: } I_0 = 2.38A$$

Thus, the measured distribution of ions can be converted into an energy distribution. This is shown for the two comparative measurements in Figure 3.3.

A maximum deviation of the intensity by about 5% of the maximum intensity was observed. Over a broader energy spectrum, the deviation is significantly smaller.
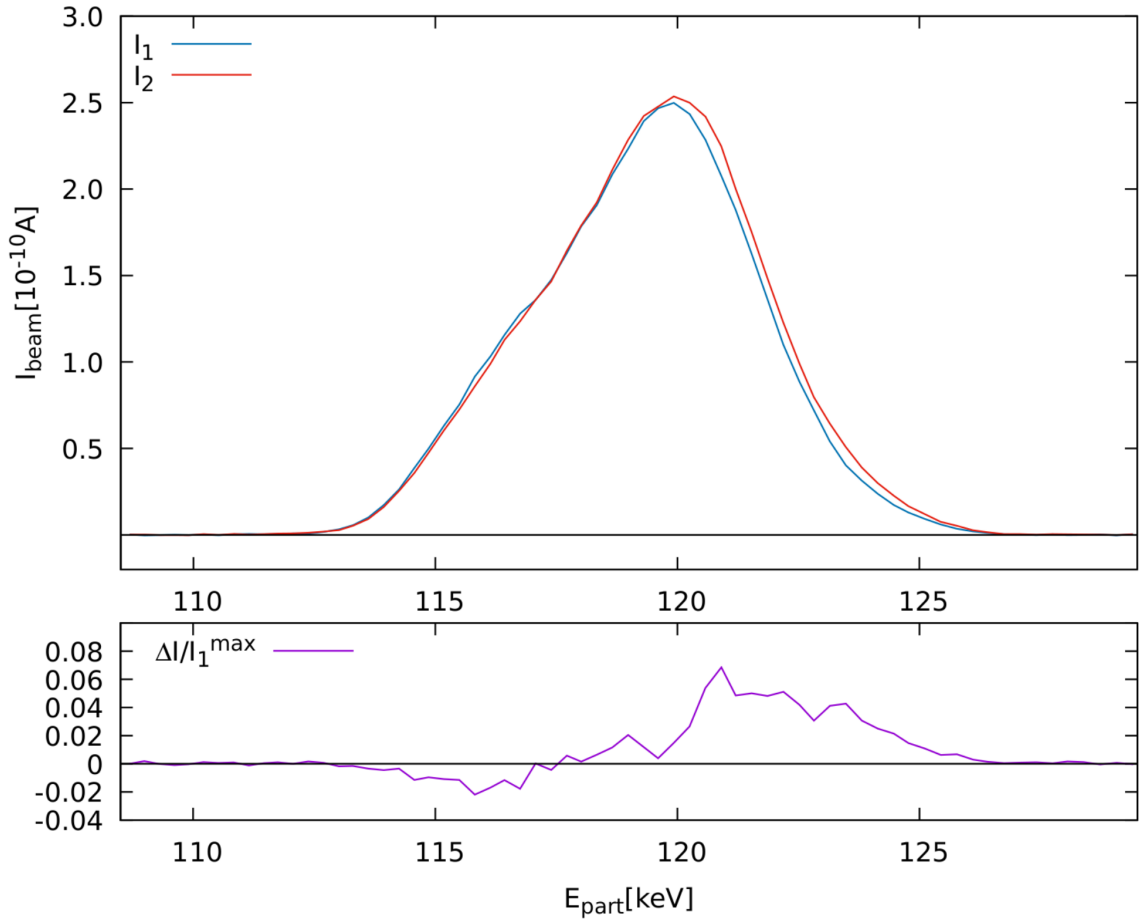

Fig. 3.3: Measurement of beam intensity as energy distribution for the selected charge state Ar^{8+} (top). Two measurements were made to verify that the beam properties remained the same. The deviation of the intensity from the maximum intensity is plotted below.

3.1.3 Charge changes in beam transport line

A large part of the beam is distributed in the selected charge state around the target energy of the accelerator. A smaller part, however, is found with a lower or higher charge state at about the same energy. This is the part of the ions which still had the "correct" charge number during extraction, i.e. received the same kinetic energy, but in the further beam transport changed their charge due to charge change processes. Other ions, which already had a different charge state before the 45° bending magnet, either from the source or due to charge changes during transport, do not arrive at the detector due to the filtering effect of the bending dipole. Therefore only the charge change processes that occured in the 45° deflected beamline are included in the discussed measurement data.

Measurement of charge changes

During detection in the spectrometer, the distributions of ions with nominal charge and ions of other charge states separate, although they have the same energy and momentum, because the ions couple to the magnetic field depending on their magnetic rigidity, i.e. depending on their charge. This is shown in Figure 3.4 for the observed charge states. Thus, provided the approximate energy of the ions is known, different charge states can be identified and the energy distributions of these different charge states can be measured independently.
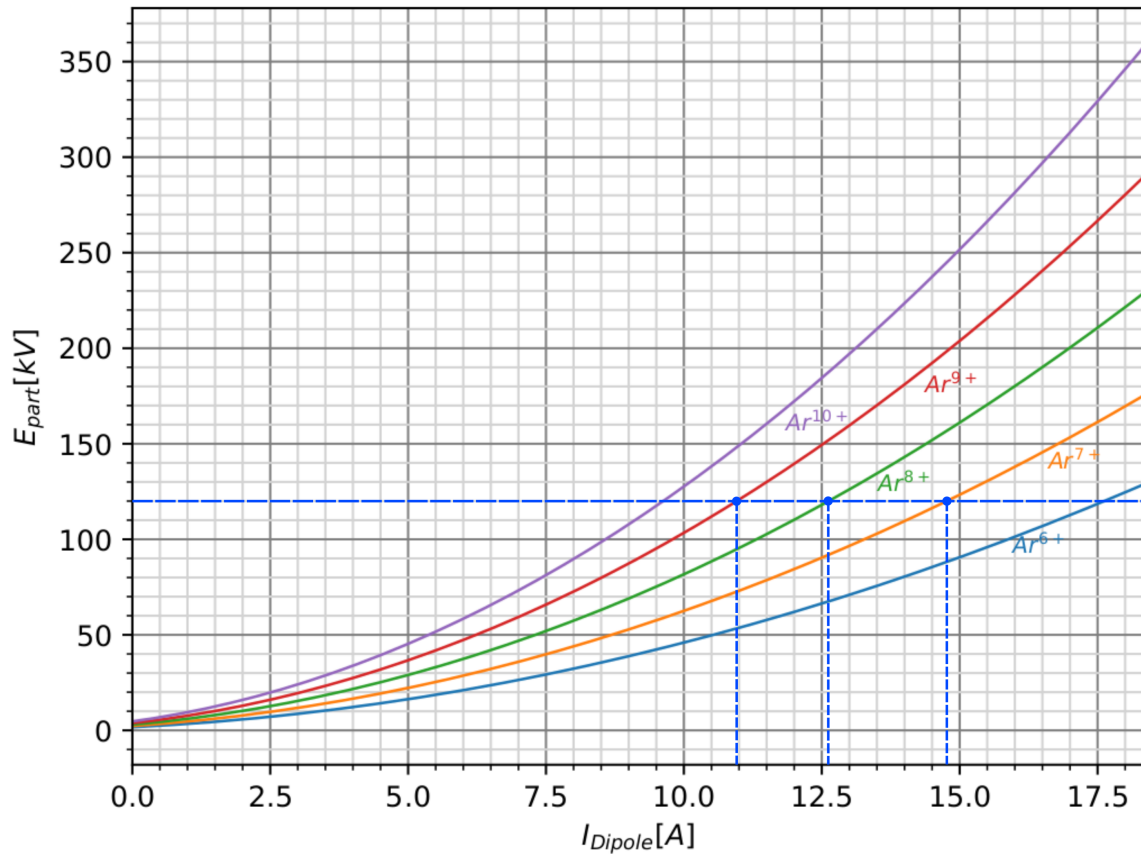

Fig. 3.4: Plot of the particle energy versus excitation current of the spectrometer for different charge states of Argon. For the charge states investigated in the experiments, their position at the used extraction energy of $120 keV$ is marked.
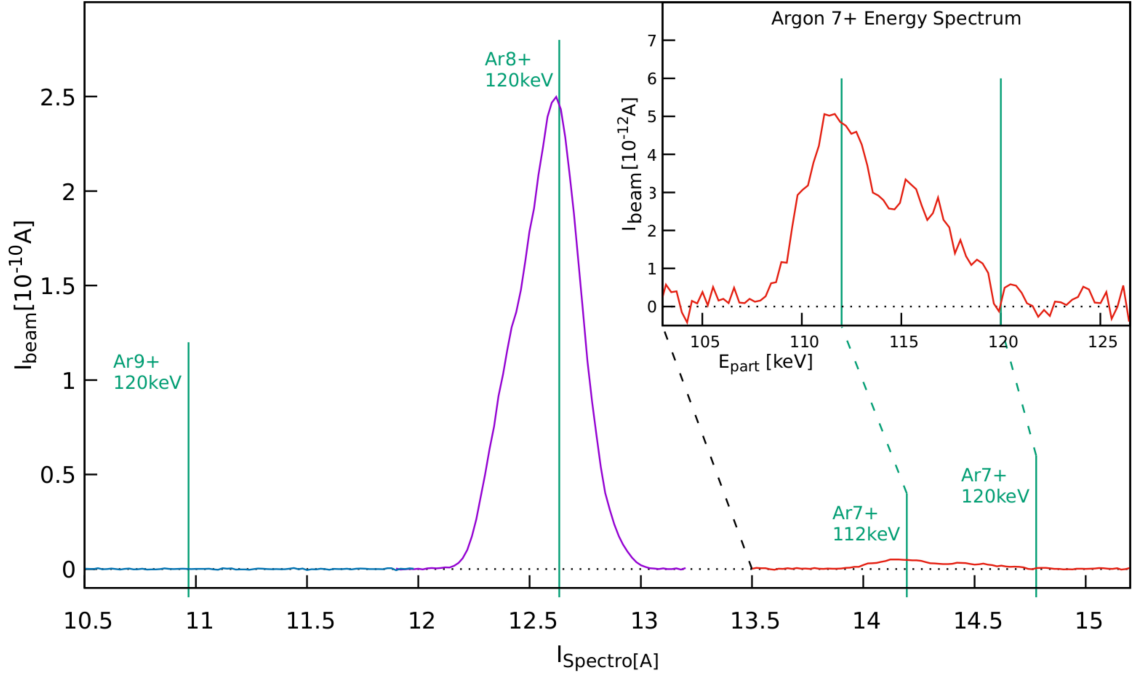
Fig. 3.5: Measurement in the range of the expected spectrometer currents for the differently charged ions. Charge changes to Ar^{9+} could not be detected (blue curve). Charge changes to Ar^{7+} are clearly visible (red curve), but very small in their intensity compared to the main charge state (purple curve). The energy distribution of the measured $Argon^{7+}$ ions is shown in the upper right.

In the measurements with the $Argon^{8+}$-beam, the spectrometer was used to identify the possible charge states Ar^{7+}, Ar^{8+}, and Ar^{9+}. As shown earlier, lower charge states are expected at higher deflection currents, higher charge states at lower currents. First, the energy distribution of the beam was measured in the target energy region (see Figure 3.3).

Subsequently, the regions where the charge states $Argon^{9+}$ and $Argon^{7+}$ are expected in the spectrometer were investigated. It was found that no measurable intensities of Ar^{9+} ions occurred. A small but clearly measurable fraction of $Argon^{7+}$ ions within the range of beam energy could be detected. These ions show a broader energy distribution than the rest of the beam and slightly lower kinetic energies. It is possible to determine from this distribution the amount of the charge change processes in the beam transport after the bending magnet. The same investigation will be performed later with the Gabor lens turned on (see section 3.3.2) to evaluate the influence of the electron cloud on recombination processes within the lens.

3.2 Spectrometry of Gabor-Lens produced ions

The energy or momentum of the ions accelerated out of the Gabor lens was measured for different settings of the Gabor lens using the momentum spectrometer. These ions do not have a specific energy, but rather a broad energy distribution. It is to be expected, however, that there is a defined upper limit to the possible energy that these ions can gain from the acceleration in the Gabor lens, since they can at most pass through the entire potential difference between anode and cathode before leaving the electric field. Such a distribution can be seen in Figure 3.6.
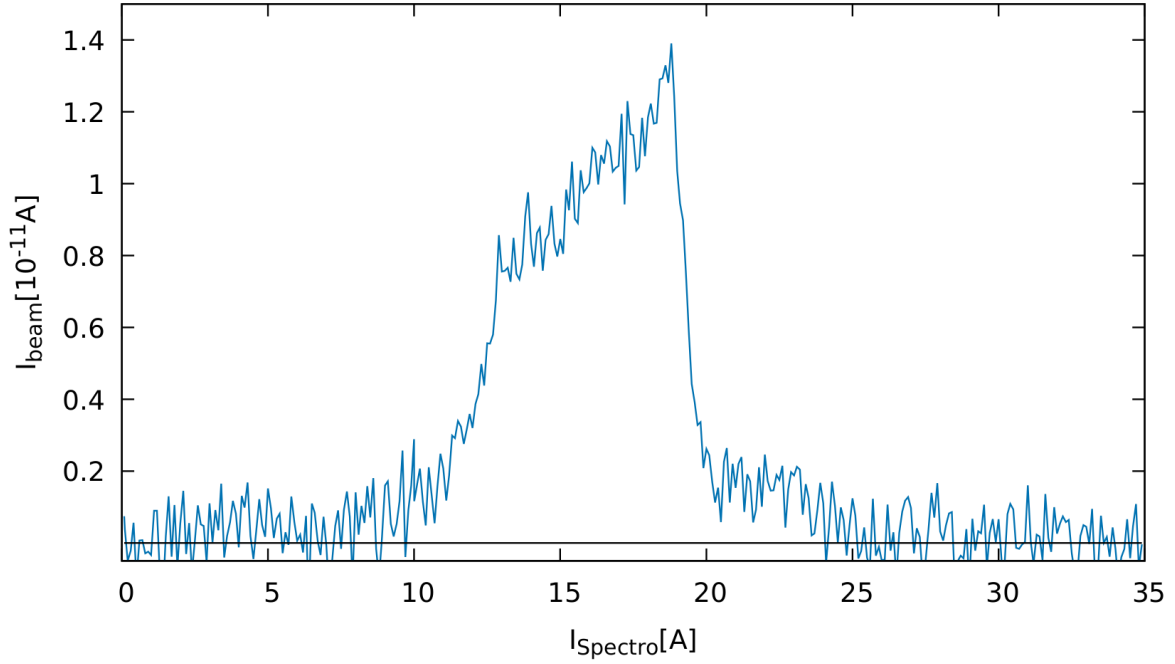
Fig. 3.6: Plot of the ion current measured in the spectrometer versus the excitation current of the spectrometer dipole at the Gabor lens setting of $\Delta\Phi = 10kV$, $I_B = 10A$. It shows a momentum distribution which grows towards higher momenta until it stops at a upper limit,seen here at an excitation current of about $19.5A$.
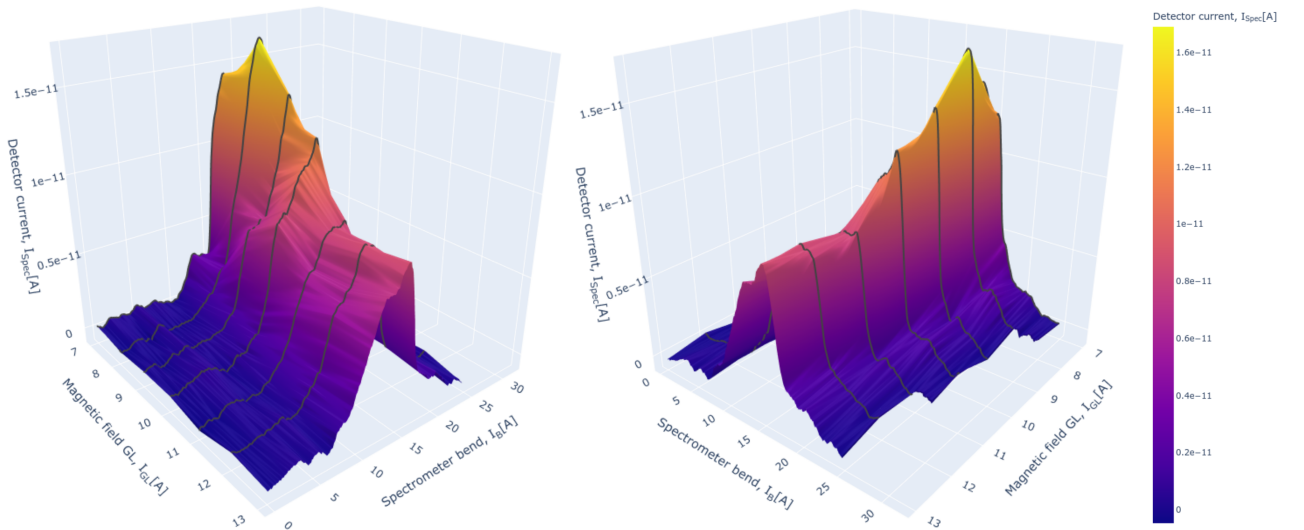

Fig. 3.7: Three-dimensional plot of the ions measured in the spectrometer emitted from the Gabor lens for different settings of the lens magnetic field. The potential was constantly set to $\Delta\Phi = 10kV$.

It shows a distribution that rises toward a peak and then breaks off at an upper limit, as expected. One can observe (see Figure 3.7) that the intensity of the measured ions reaches a narrow peak at low magnetic fields, whose maximum intensity is stronger compared to higher field strengths, where the
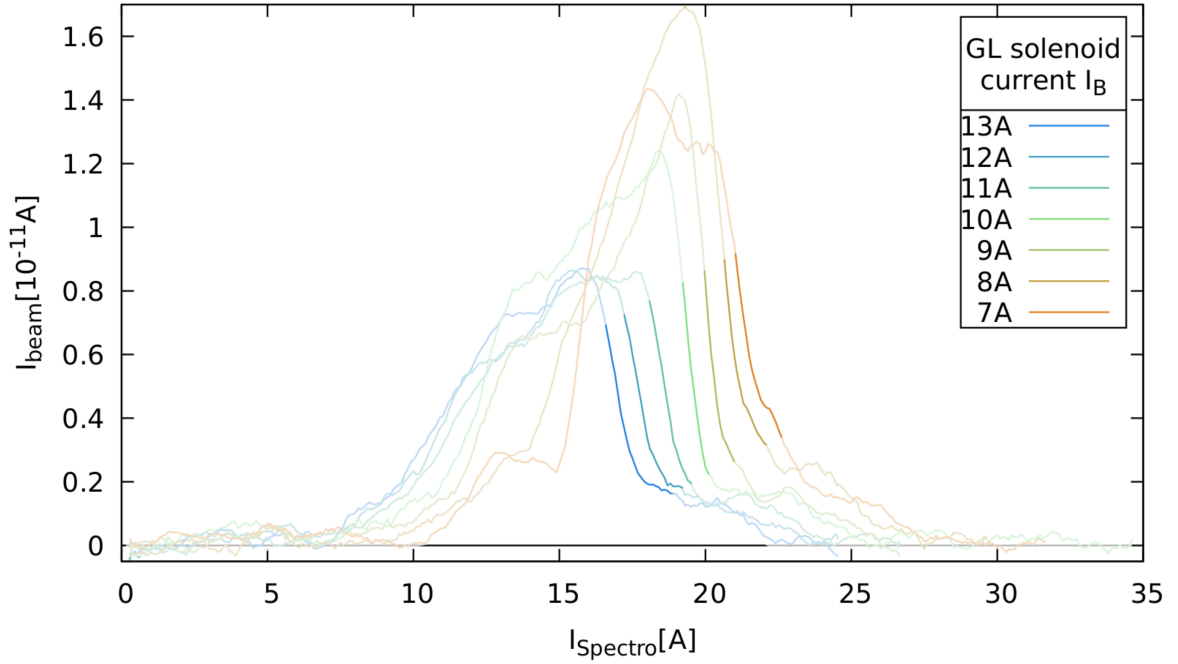
34

Fig. 3.8: Overlay of ion distributions for different settings of the magnetic field of the lens at a potential setting of $\Delta\Phi = 10kV$ with a residual gas pressure of $p_0 = 6 * 10^{-7} mbar$. Highlighted is the region of the cutoff edge, which shifts to the left (to lower momenta) with increasing magnetic field.

distribution broadens. This implies a different momentum distribution of the measured ions from the Gabor lens for different settings of the magnetic field. It is possible that the ions produced actually have different momentum distributions. Thus, their momentum depends mainly on the production region within the lens, since depending on it they pass through only a part of the accelerating electric field.

On the other hand, the maximum momentum, i.e. the clearly recognizable cutoff edge of the momentum distribution at the upper limit, depends on the filling degree of the Gabor-Lens and therefor the resulting compensation of the electric potential inside the lens. A high filling level, which means a dense electron cloud inside the lens, leads to a compensation of the positive potential in the center of the lens by accumulation of negatively charged electrons. As a result, the maximum potential difference passed by ions accelerated out of the lens is smaller, thus their momentum is lower. Consequently, from the position of this upper momentum limit, the filling level of the lens can be deduced. In Figure 3.8 one can see how the upper momentum limit continuously decreases with increasing magnetic field, i.e. how the maximum momentum of the particles decreases due to better filling of the lens. More comprehensive measurements have already been carried out by Klaproth[8], both on the filling level and the spectra influenced by it, and on the production areas within the lens. Further, maps describing the state of the lens depending on its setting have been produced by varying both the potential and the magnetic field.

Future studies with the setup now used can repeat these measurements with an ion beam propagating through the lens, separating the spectrum of the beam and the ions emitted from the Gabor lens by adjusting the beam energy appropriately to gain insight into the effect of the beam on the state of the electron cloud.

3.2.1 Investigation on emitted particle mass

To convert the measured excitation currents of the spectrometer dipole into particle energies, the mass and charge of the ions must be given. Since these are not always known (unless a specific gas was introduced), but it must hold that the energy distribution of the ions breaks off at the upper energy limit of the accelerating potential $E^{max} = e \cdot \Phi_{Acc}^{max}$ (for singly charged ions), the mass of the ions can be determined from this limit (and with the fact that the ions have integer mass and charge numbers). In Fig. 3.9 the conversion to energies is plotted for the distribution shown earlier (Fig. 3.6), for different possible masses and charges. Since the Gabor lens was operated here without introducing any particular gas, the gases that make up the majority of air were assumed to be the source of the possible ions.
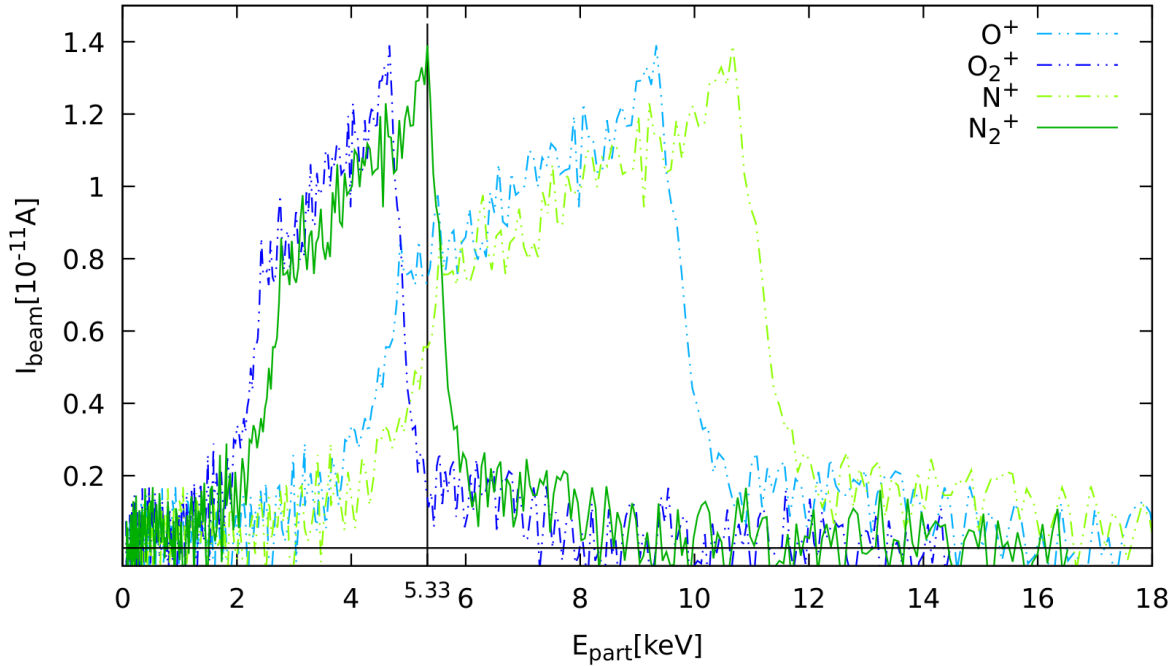

Fig. 3.9: Plot of the conversion to an energy distribution for possible ion species (contained in the vacuum residual gas). It can be seen that only the distributions of N_2^+ and O_2^+ fit the expected energies.

Taking into account that the ratio of accelerating potential to anode potential $\frac{\Phi_{Acc}}{\Phi_{Anode}}$ must be much smaller than 1 due to the filling of the lens, the ions are expected at energies of $0 < E^{max} << q \cdot 10 kV$. It turns out that the majority of the measured ions from the Gabor lens can be doubly charged oxygen or nitrogen molecules (see Figure 3.9). Since the largest fraction of the residual gas is nitrogen, which also determines the upper limit of the distribution, it can be assumed that the main part od the measured distribution is given by nitrogen in the N_2^+ state. The upper limit of possibly lower intensity O_2^+ molecules is below the excitation currents at which the nitrogen distribution is visible.
For the ionized nitrogen N_2^+ molecules, the maximum energy in this distribution is $E^{max} \approx 5.3 keV$.

3.2.2 Analysis of Spectra with known particle kind

In further measurements, helium was introduced into the vacuum to observe gas ions of known mass in the spectrum.
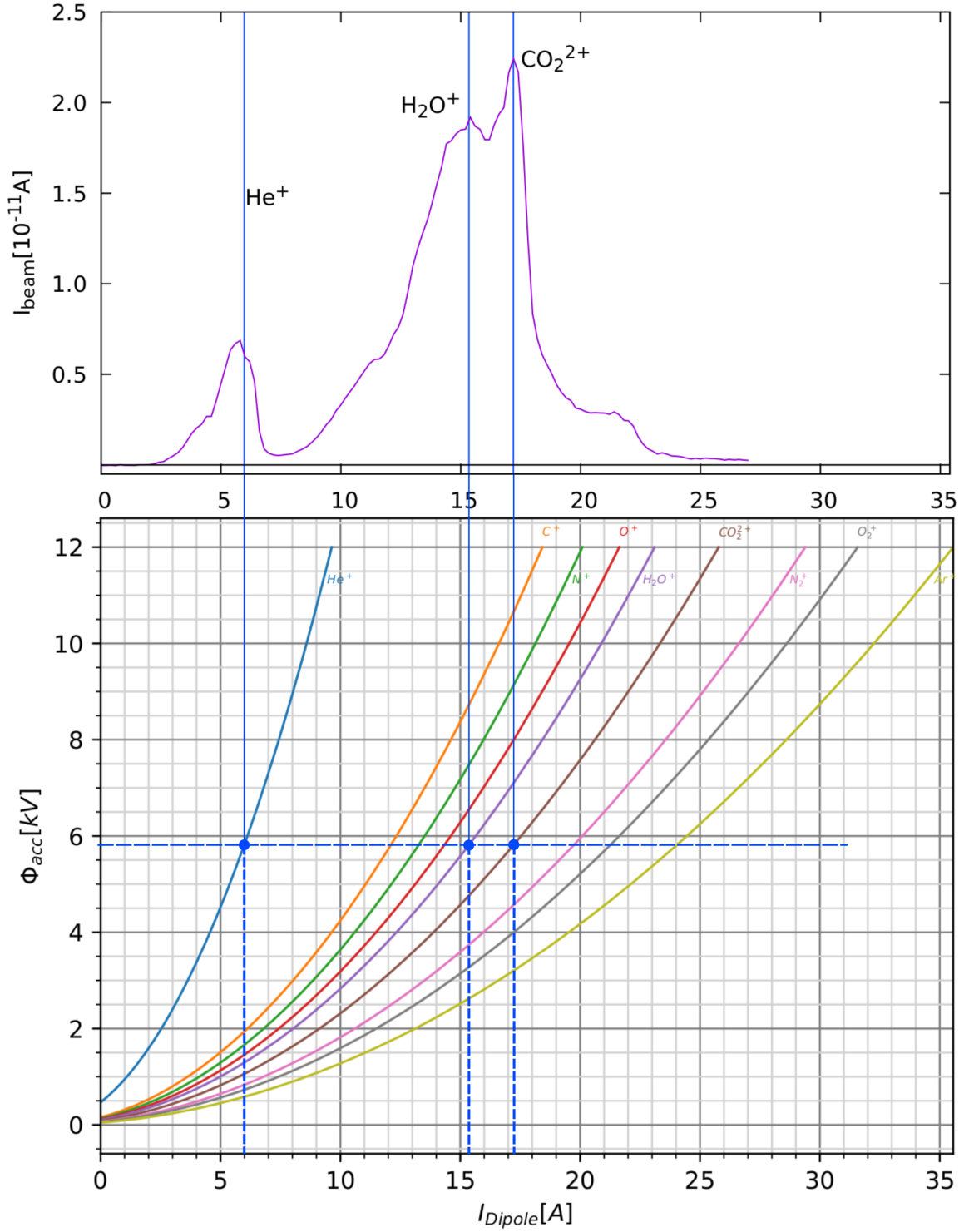
Fig. 3.10: Plot of the spectrum with introduced helium at a pressure of $p = 5 \cdot 10^{-5} mbar$ and the setting of the lens: $\Delta\Phi = 10kV$, $I_B = 10A$. Above, the full spectrum with the peak of helium as reference on the left and the other two observed peaks on the right. Below a plot of the accelerating potential versus the expected excitation current for deflection in the spectrometer for different particles and states.

The pressure was increased from about $p_0 = 6 \cdot 10^{-7} mbar$, which can be achieved in the setup so far,

to $p_{He} = 5 \cdot 10^{-5} mbar$. Figure 3.10 shows the spectrum of the emitted ions while introducing helium after several weeks out of service without subsequent extensive conditioning.

A clearly identifiable peak of introduced helium appears in the spectrum, from which one can determine the peak energy of the emitted ions. With this, the filling level of the Gabor lens can also be determined. For the measured energy of $E_{He+} \approx 5.8 keV$ this implies an accelerating potential of about $\Delta\Phi = 5.8kV$, while the anode potential was set to $\Delta\Phi = 10kV$.

Thus the filling level results from the compensation of the anode potential:

$$\frac{\Phi_{Anode} - \Phi_{Acc}}{\Phi_{Anode}} \approx 42\%$$

In addition, the peaks of further ions can be seen. Since the energy of all produced ions depends on the accelerating potential or the filling degree of the lens, it can be assumed that the other observed ions were accelerated in the same potential. Thus, the ratio m/q or A/Z for these ions can be determined from the excitation currents associated with the peaks.

For the left of the two high peaks (see Figure 3.10), $A/Z \approx 18$ is found. This indicates singly charged water molecules.

For the right peak, $A/Z \approx 22$ is obtained, which does not apply to any singly charged molecule occurring in the atmosphere. In fact, however, the metastable state of carbon dioxide CO_2^{2+} lies at this mass-to-charge ratio which can be produced by electron impact ionization as was observed by Straub et al.[9]. Lifetime measurements of this state have yet shown differing results [10].

The presence of both water and carbon dioxide can be related to desorption of the attached molecules from the wall. The intensity of these ions in the spectrometer is higher than the intensity of helium, but this is not a direct indication of the production rate in the lens, since helium, due to its lower mass, reacts more strongly to space charge of the emitted ions and therefore, after transport to the spectrometer, is found in lower intensities within the aperture of the spectrometer than heavier ion species.

Further measurements in the future can verify whether the observation on CO_2^{2+} is confirmed and, going forward, the properties of this state can be analyzed.

3.3 Influences of Gabor-Lens on charged particle beam

3.3.1 Effects of Gabor-Lens structure

As a reference, before measuring the influence of the activated Gabor lens on the beam, the influence of the individual elements of the Gabor lens on the beam spectrum was first investigated. As described, the arrangement of the electrodes acts like an electrostatic einzel lens. First, a reference spectrum without potential and magnetic field was acquired. Subsequently, the potential and the magnetic field were set individually to a usual value for the operation of the lens and the spectra of the beam were measured again.

Influences on the beam spectrum

The spectra remain similar with respect to the energy distribution. However, it can be clearly seen that the maximum intensity is significantly higher when the magnetic field of the lens is switched on. When the potential is switched on, the intensity is slightly reduced.

A possible explanation for the increase in intensity is weak focusing of the solenoid, which could focus the beam into the aperture of the spectrometer.
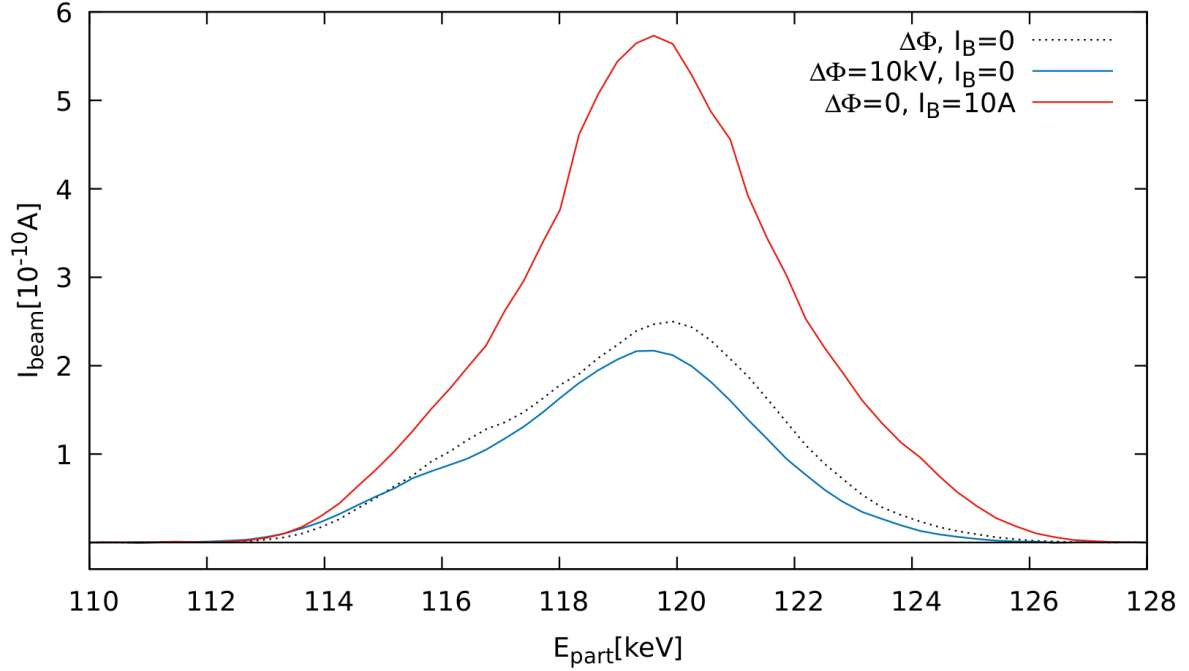
Fig. 3.11: Diagram of the beam spectrum in the main charge state under the influence of the setting of the potential (blue) and the magnetic field (red) of the Gabor lens. An influence of the elements of the Gabor lens on the beam optics can be clearly seen.

Though, for the intensity when the potential is switched on, a slight increase would also have to occur due to the focusing effect of the electrostatic einzel lens. Since this is not the case, it can be assumed that space charge forces in transport also play a role.

Thus, space charge compensation due to electron capturing in the beam potential is aided by axial confinement in the magnetic field of the lens. In contrast, in the case of the switched-on potential, electrons are pulled out of the beam toward the potential of the anode, so that space charge compensation is absent for further transport. In the absence of space charge compensation, the focus, which was previously set with the quadrupole triplet, shifts to longer focal lengths (focus shift). Thus, the intensity at the aperture of the spectrometer decreases.

Also visible is a slight shift of the peak of the distribution towards smaller energies. However, since the elements used (einzel lens and solenoid) cannot lead to any energy variation of the ions, it can be assumed that the measurement of the energy was slightly distorted. This means that the beam enters the spectrometer at an angle and thus the radius of the circular path that an ion describes to enter the Faraday cup in the deflection direction is slightly varied. This effect could be caused by a misalignment of the Gabor lens with respect to the spectrometer or with respect to the beam axis, both by a transverse shift or a slight rotation of the lens axis with relation to the beam axis.

Effects on charge changes

In the region of the spectrum where Argon-7+ was previously observed, the spectrum was now examined again. Under the influence of the magnetic field of the lens, it can be seen that the distribution takes a different shape (see Figure 3.12). In particular, it can be seen that the peak of the distribution appears to be greatly reduced, i.e. fewer Ar^{7+} ions arrive in the spectrometer, especially in an energy range where most of this charge state previously occurred. The cause of this has not yet been

investigated in detail.

Possibly, an increased length of the ions' path through the residual gas inside the lens, caused by the magnetic field of the solenoid, leads to an increase of the probability of further recombination processes. Then possibly a redistribution to even lower charge states, especially Ar^{6+} may occur.

Future measurements can show how the spectrum will look like in the region of these doubly recombined Ar^{6+} ions and whether indeed higher intensities occur there under the influence of the solenoid field.

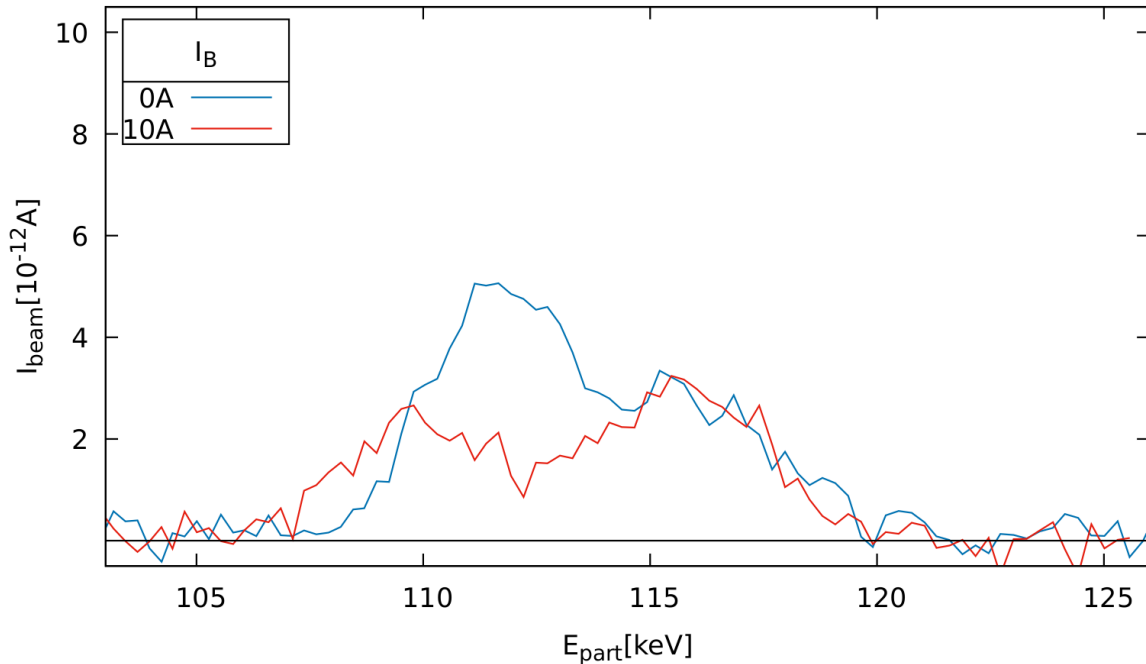Setting the potential of the lens in the configuration as an electron trap, i.e. with positive potential

Fig. 3.12: Energy spectrum of ions charged to Ar^{7+} at varied current through the solenoid of the Gabor lens, where the potential was left at $\Delta\Phi = 0$.

of the anode in the center of the lens with respect to the outer space, the beam ions are decelerated when entering the lens and accelerated again when leaving, so that no change of energy occurs. This influence is very large especially relative to the very low particle energies ($15kV$ accelerating voltage, lens potential $\sim 10kV$). The lower particle energy inside the lens respectively the increased time of flight increases the probability for recombination with free electrons inside this region. Ions that recombine inside the lens and therefore are less charged lose energy because they are decelerated more at the entrance than they are accelerated with lower charge at the exit. For the selected beam energy (extraction voltage of the source $15kV$ and q=8e), a potential setting of the lens of $10kV$ and the charge change from Ar^{8+} to Ar^{7+} results:

$$E_{part} = q \cdot U_{ext} = 120keV$$
$$E'_{part} = E_{part} - W_{Stop} + W_{Acc} = E_{part} - 8e \cdot 10kV + 7e \cdot 10kV = 110keV$$
$$or \Delta E = 10keV$$

Therefore, the expectation is that the distribution of the spectrum of the lower charged ions will divide into two energy regions, thereby distinguishing charge changes occurring inside and outside the lens.
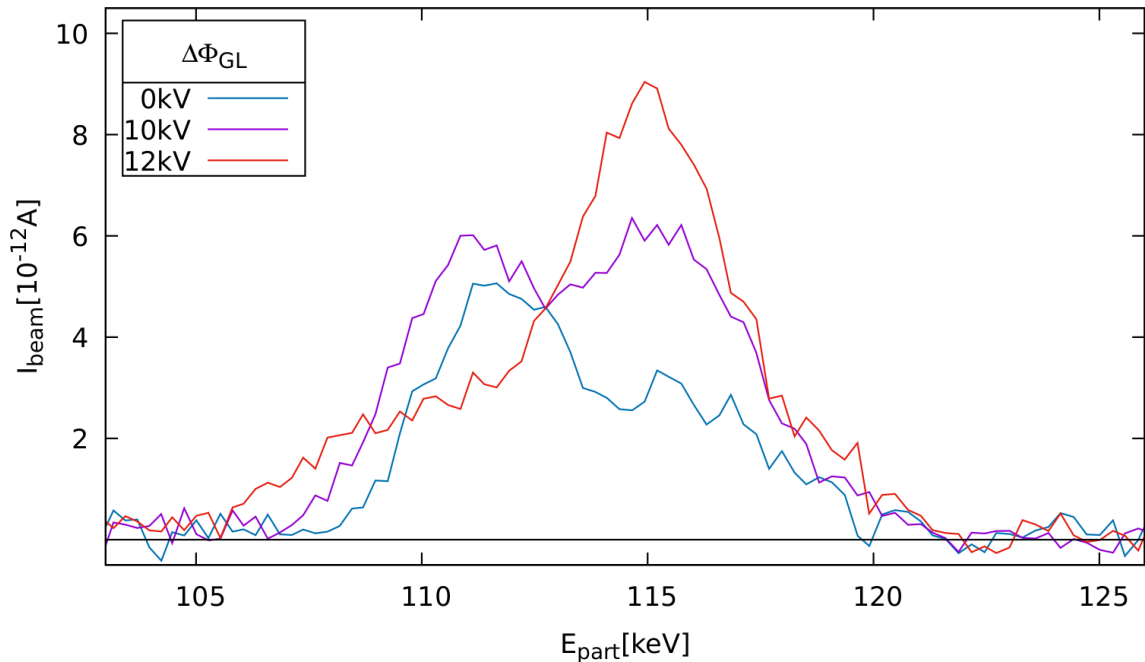
Fig. 3.13: Energy spectrum of ions charged to Ar 7+ at varying potential of the Gabor lens, whereby the solenoid was left without current.

In fact, the measurements showed a splitting of the original spectrum into two peaks (see Figure 3.13). At a set lens potential of $10kV$, two peaks of the distribution show up at about the same height as before in the spectrum of the unaffected beam. This is consistent with expectations in that the described partitioning is observed and the total number of charge changes increases. However, it can also be seen from the spectrum that the additional peak of the distribution is shifted to a slightly higher energy. This contradicts the assumption that less energy is gained on exiting the lens due to the reduced charge state. To check this, another spectrum was recorded at higher potential. Then the peak located at higher energies continues to increase, while at lower energies the distribution flattens out. This seems to verify that the charge changes occurring within the lens indeed lead to ions at higher energy, since at higher potential the recombination probability increases. This will require further measurements in the future that will provide more detail as to why this energy shift occurs.

3.3.2 Effects of electron plasma cloud

The influence of the activated Gabor lens on the beam spectrum was now investigated. The Gabor lens was operated with the same settings for potential and magnetic field, of which the influence on the beam spectrum had previously been measured individually. The spectrum of the two expected charge states 7+ and 8+ was measured.

Effects on the main charge state

With respect to the spectrum of Ar^{8+} ions, two effects are visible: First, the distribution of the beam ions becomes narrower during transport through the Gabor lens, i.e. the totality of the beam ions is found in a narrower energy range. Additionally, the peak intensity increases. Secondly, the distribution seems shifted to higher energies overall. Since no accelerating influence of the Gabor lens
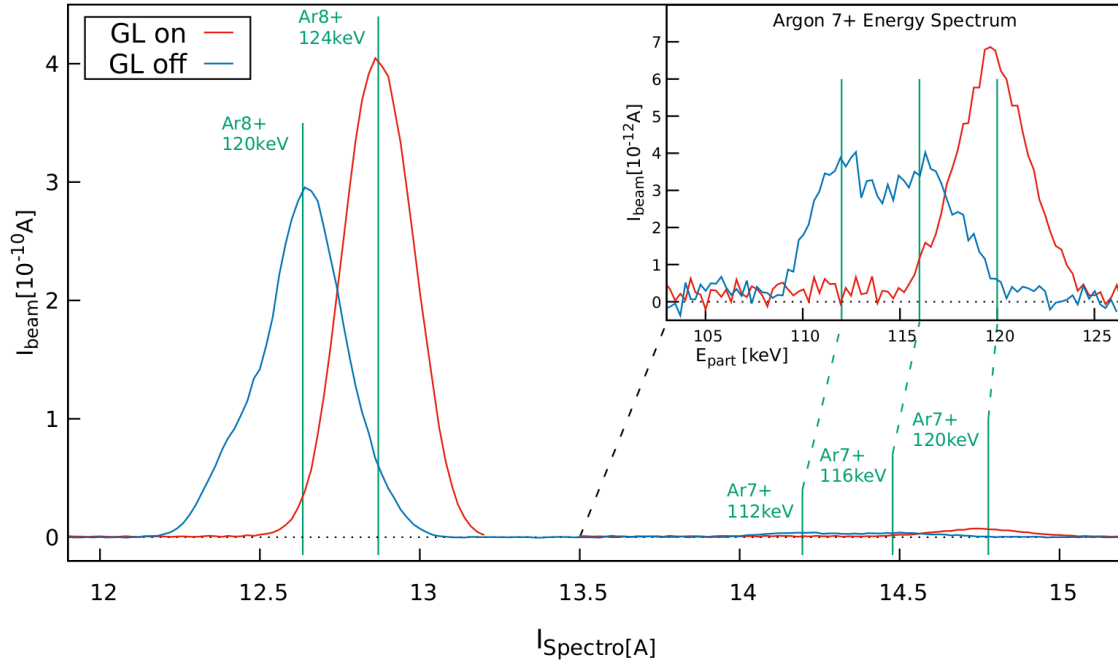
Fig. 3.14: Spectrum of the beam both without and with the influence of the Gabor lens. The energy spectrum for the 7+ charge state is shown at the top right.

is to be expected, this is probably again a deflection of the beam with respect to the original beam axis. With the lens activated, this effect is now much more visible and occurs in reverse orientation. Furthermore, since this effect causes a different "slice" of the beam to be detected by the aperture of the spectrometer, this may also explain why the intensity and width of the energy distribution vary. These results suggest that in the future, realigning the Gabor lens or spectrometer combined with fine-tuning the beam direction with the bending dipole may lead to better results.

Effects on charge changes

A special interest in the use of the spectrometer for investigations concerning the influences of Gabor lenses on ion beams lies in the consideration of the charge change processes within the lens. Since an electron cloud is generated there through which the beam propagates, it is an obvious first assumption that an increased number of recombinations of beam ions with these electrons occurs. However, since the recombination cross sections are very small at high relative velocities, there is also the assumption that the influence of the electron cloud is negligible. Instead, the number of recombination processes could even decrease, since the most probable process is a three-body recombination, which requires additional collision partners to carry away the excess energy in the collision. However, since inside the lens the density of ions is not exactly known and (since the ions produced there are accelerated out of the cavity) may even be lower than outside the lens, there may be a lack of collision partners inside the lens for that. To clarify this, the measured spectrum with the Gabor lens switched on was now compared to that without the Gabor lens. In order to be able to determine the rate of charge changes, the total number of measured ions per time with the charge state 8+ was first determined for both distributions by integrating the measured spectrum (see Figure 3.15).
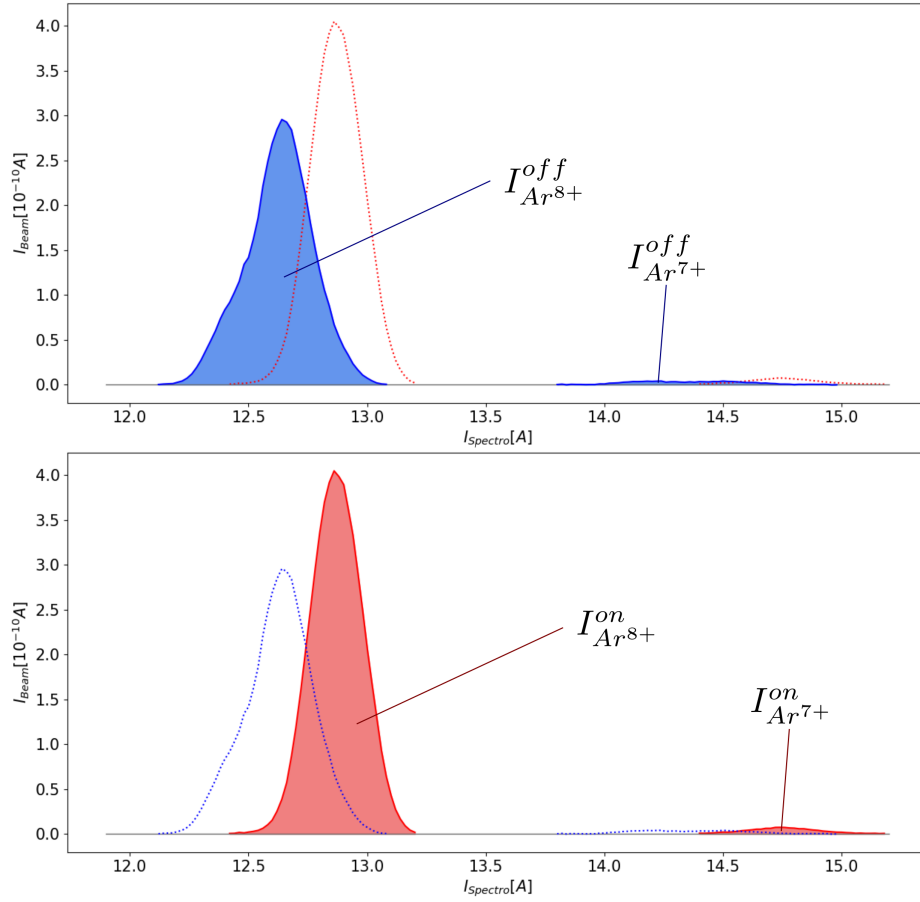
Fig. 3.15: Determination of the total number of ions by integration for the different regions in the spectrum allowing the charge states Ar^{8+} and Ar^{7+} to be considered separately.

It results:

$$\dot{N}_{Ar^{8+}}^{aus} = \frac{1}{8e} I_{Ar^{8+}}^{aus} = 7.54 \cdot 10^7$$

$$\dot{N}_{Ar^{8+}}^{an} = \frac{1}{8e} I_{Ar^{8+}}^{an} = 8.70 \cdot 10^7$$

Then, the number of Ar^{7+} ions per time was determined by the same method:

$$\dot{N}_{Ar^{7+}}^{aus} = \frac{1}{7e} I_{Ar^{7+}}^{aus} = 2.00 \cdot 10^6$$

$$\dot{N}_{Ar^{7+}}^{an} = \frac{1}{7e} I_{Ar^{7+}}^{an} = 2.32 \cdot 10^6$$

The ratio of charge changes can then be calculated for both cases.

$$n^{aus} = \frac{\dot{N}_{Ar^{7+}}^{aus}}{\dot{N}_{Ar^{8+}}^{aus}} = 2.65\%$$

$$n^{an} = \frac{\dot{N}_{Ar^{7+}}^{an}}{\dot{N}_{Ar^{8+}}^{an}} = 2.67\%$$

It is found that the rate of charge changes when the Gabor lens is active is not significantly different from the value when the lens is inactive.

Chapter 4

Conclusion and outlook

The measurements on the Argon[8+]-beam have, in addition to the beamline setting and the energy spectrum of the beam, provided the first results on the rate of charge change processes in the beamline. The studies performed on the Gabor lens have shown the acquisition of spectra of the ion production in the Gabor lens and the calculation of the filling level based on known particle species. In the combination of switched-on Gabor lens and ion beam, the rate of charge changes was also determined and no significant increase was found compared to switched-off lens. Apart from that, the measurements in combination with the ion beam suggest that precise realignment of the Gabor lens spectrometer section with respect to the beam will result in a better straight line hit of the beam into the spectrometer with the Gabor lens on.

Further research regarding the production locations of the ions within the lens can be done to subsequently investigate the properties of the electron cloud interacting with an ion beam. For this purpose, measurements can be made at different settings of the lens and then repeated with the ion beam. The energy of the beam must then be chosen in such a way that the spectra of the Gabor lens and the ion beam are clearly separated. For this purpose and for further energy variation of the beam in other measurements, e.g. regarding the energy dependence of the charge change processes, the RFQ can be put into operation in the future and provide variable particle energies for the measurements as described.

The expected particle species were found in the Gabor lens spectra, but also ions with a mass-to-charge ratio $A/Z = 22$, suggesting the presence of doubly charged carbon dioxide molecules. The suggestion of ionization of carbon dioxide released by desorption to CO_2^{2+} can be revisited in the future after an addtional shutdown time of the lens. Further, by introducing CO_2 into the lens, controlled conditions can be created to study the production of this state in more detail without interference from other ions. It would also be interesting here to see if the decay of this metastable state to $CO^+ + O^+$ or $C^+ + O_2^+$ also becomes visible in the spectrum.

With further measurements at different settings of the lens and at different beam energies and later on, if necessary, the application of other measurement methods (e.g. with an energy spectrometer), insights can be gained as to why the expected splitting of the spectrum of the recombined ions of the beam was observed contrary to the expected energy shift.

Bibliography

[1] H.Schmidt-Böcking A. Schempp et al. "The Frankfurt ECR-RFQ Ion-Beam Facility for Slow Highly Charged Ions". *Materials Research with Ion Beams*. Ed. by Prof. Dr. Horst Schmidt-Böcking and Priv. Doz. Dr. Alwin Schempp. Springer-Verlag, 1992, pp. 71–83.

[2] S Biri et al. "Developments and Plasma Studies at the ATOMKI-ECRIS". *AIP Conference Proceedings* 749.1 (Mar. 2005). ISSN: 0094-243X. DOI: 10.1063/1.1893368. URL: https://www.osti.gov/biblio/20630695.

[3] D. Todd D. Leitner et al. "USPAS - Fundamentals of Ion Sources 8./9. Electron Cyclotron Resonance Ion Sources". U.S. Particle Accelerator School (2016).

[4] F. Hinterberger. *Physik der Teilchenbeschleuniger und Ionenoptik*. Springer, 2008.

[5] T. Dönges. "Entwicklung eines Kontrollsystems für den manuellen und automatisierten Betrieb von Raumladungslinsen". Goethe Universität Frankfurt am Main, Institut für Angewandte Physik, 2021.

[6] F. Plag. "Feldmessungen am Dipolmagnet und deren Vergleich mit Simulationsrechnungen". Goethe Universität Frankfurt am Main, Institut für Angewandte Physik, 2010.

[7] C. Krause. "Optimierung des ultrastabilen rauscharmen Stromverstärkers". PhD thesis. Technische Universität Braunschweig, Institut für Elektrische Messtechnik und Grundlagen der Elektrotechnik, 2019.

[8] S. Klaproth. "Development of a Control System for Space Charge Lenses based on Experimental Data". Goethe Universität Frankfurt am Main, Institut für Angewandte Physik, 2017.

[9] H. C. Straub et al. "Absolute partial cross sections for electron-impact ionization of CO2 from threshold to 1000 eV". *The Journal of Chemical Physics* 105.10 (1996), pp. 4015–4022. DOI: 10.1063/1.472275.

[10] Andrew Slattery et al. "Spectroscopy and metastability of CO22+ molecular ions". *The Journal of chemical physics* 122 (Mar. 2005), p. 84317. DOI: 10.1063/1.1850895.